A Study on an Active Magnetic Bearing Control

능동 자기 베어링의 제어에 관한

연구

A Study on an Active Magnetic Bearing Control

A Dissertation
by
Yu Chang
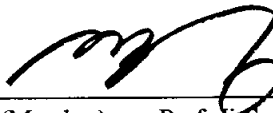
Approved as to style and content by:

(Chairman)   Prof. Byung-Gun Jung
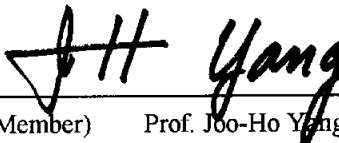

(Member)   Prof. Seok-Kwon Jeong

(Member)   Prof. Ji-Seong Jang

(Member)   Prof. Young-Bok Kim

(Member)   Prof. Joo-Ho Yang

February, 2004

常宇 의 공학박사 학위논문을 인준함

2003년 12월 26일

주　심　　공학박사　정　병　건

부　심　　공학박사　정　석　권

위　원　　공학박사　장　지　성

위　원　　공학박사　김　영　복

위　원　　공학박사　양　주　호

Contents

Figures List

Table List

Nomenclature

a_1, a_2: the amplitude of mode1 and mode 2 respectively in flexible model of the rotor

A: flexible body system matrix

A_c: state space matrix of closed-loop system

A_o: state space matrix of observer in the closed-loop system

A_r: rigid body system matrix

A_s : the cross-sectional area of the magnet [m^2]

B: flexible body input matrix

B_r: rigid body input matrix

C_{a2b}, C_{a2s}: the dynamic matrix from the amplitude to the displacement at bearing position and sensor position

C: flexible body output matrix

C_r: rigid body output matrix

D: direct term

F_l, F_r: force of left and right bearing [N]

g: the gap between the electromagnet and rotor [m]

$G(s)$: transfer function of plant

$G_{11}, G_{12}, G_{21}, G_{22}$: transfer functions of electromagnet

i_{cl}, i_{cr}: current on left and right electromagnets [A]

I : coil carrying current in the magnet [A]

I_0 : the mass moment of inertia of the shaft for x axis or y axis[$kg \cdot m^2$]

J: performamce index

k_{mx}: displacement gain

k_{mt}: slope gain

K: SVFB gain (in chapter 4); controller (in chapter 5)

$K_1(s)$: transfer function of the displacement controller

$K_2(s)$: transfer function of the slope controller

K_{dx}: displacement speed gain

K_{dt}: slope speed gain

K_p: proportional parameter

K_{px}: displacement parameter

K_{pt}: slope parameter

l_1: the distance from the rotor mass center to the bearing [m]

l_3: the distance from the rotor mass center to the sensor [m]

L: electromagnets coil inductance [H] (in chapter 2)

L: observer gain matrix (in chapter 4)

m: rotor mass [kg]

M_{s2b}, M_{s2s}: dynamic matrix from the states to the displacement at bearing position and sensor positaion

N : the number of coil in the magnet

P: the nominal plant of flexible system (in chapter 2)

P: SVFB auxiliary matrix (in chapter 4)

P_{11}, P_{12}, P_{21}, P_{22}: transfer functions of nominal plant

P_o: observer auxiliary matrix

Q, R: weighting matrices in the performamce index

Q_o, R_o: observer design matrices

r: external disturbance signal

R : force-displacement coefficient [N/m]

R_I: current amplifier resistance[Ω]

R_L: eletromagnets coil resistance[Ω]

S : force-current coefficient [N/A]

T_d: differential parameter

u: control input vector

u_1, u_2: control input vectors on left and right side [V]

u_x: control input vectors of displacement [V]

u_t: control input vectors of slop [V]

v: new command input vector

V_{cl}, V_{cr}: outputs on left and right side of controller [V]

V_{sl}, V_{sr}: outputs on left and right side of sensor [V]

w: external disturbance to the $\mathcal{H}_\infty$ control system

w_t : complementary sensitivity weighting function

w_s : sensitivity weighting function

W_T: complementary sensitivity weighting matrix

W_S : sensitivity weighting matrix

W_2 : control input weighting matrix

x: state vector of plant

x_r: state vector of rigid rotor

x_0: the horizontal displacement at the mass center of the rotor [m]

x_{bl}, x_{br}: the horizontal displacement at the points of left and right bearing [m]

x_{sl}, x_{sr}: the horizontal displacement at the points of left and right sensor [m]

u_{xl}, u_{xr}: control input at left and right bearing position[V]

$\hat{x}$: estimative state vector in observer

$\tilde{x}$: state estimation error

y: output vector

y_r: output vector with the rigid rotor

y_1, y_2: output vector on left and right side

z_1, z_2, z_3: output of the $\mathcal{H}_\infty$ control system

γ: tuning parameter in sensitivity weighting matrix

Δ_m: multiplicative uncertainty

a : current amplifier electromagnets coil gain [Ω /H]

β : coefficient of displacement/voltage relation of sensor [V/m]

θ : the horizontal angle from rotor axis to the system z axis in counter clockwise [rad]

μ_0 : permittivity of free space [N/A^2]

λ : the control voltage proportional to the other side

κ_1 : displacement-force coefficient of bearing [N/m]

κ_2 : current-force coefficient of bearing [N/A]

초록

능동 자기 베어링(Active Magnetic Bearing : AMB)은 회전축을 전자기력에 의해서 완전 비접촉으로 지지하는 기계 요소이다. 자기 베어링은 회전축과 지지 요소가 비접촉이기 때문에 일반적으로 널리 쓰이고 있는 접촉식 베어링과는 달리 마찰, 열, 소음이 거의 없다. 따라서, 베어링 메탈의 마멸, 진동과 소음의 발생, 윤활 및 그 냉각 장치를 구비해야 하는 등의 기계적 접촉식 베어링이 갖는 문제점들을 해결할 수 있다. 또한, 자기 베어링은 기계식 베어링에 비하여 지지 면적이 크므로 지지력이 분산·평균화되고 부드럽게 지지할 수 있다. 뿐만 아니라 지지 강성 및 댐핑을 바꾸거나 혹은 로터의 동특성을 모니터링하거나 하는 고도의 기능을 갖게 할 수 있으므로 이른바 꿈의 베어링이라고도 부르고 있다.

능동 자기 베어링에 관련된 기술은 매우 복잡할 뿐더러 배경 이론의 불충분으로 인하여, 국내외적으로 많은 연구가 진행되고 있다. 현재 진행되고 있는 연구는 주로 AMB 의 응용영역의 확장과 기존 베어링의 제어 성능향상으로 분류할 수 있는데, 본 연구는 기존의 자기 베어링 시스템의 제어 성능 개선을 목적으로 한다.

구체적으로 미국 Magnetic Moment, LLC 사의 'MBC 500' 이라고 명명된 자기 베어링 시스템을 제어 대상으로 하고, 이 제어대상에 관하여 세 가지의 모델링을 하였는데, 첫번째는 로터를 강체로 간주하여 모델링하였고, 두번째는 로터를 플렉시블 축계로서 상태공간 모델링하였으며, 세번째는 플렉시블한 축계로 간주하여 모델링된 시스템을 저차모델로 저차원화된 공칭 모델을 구하였다. 제어대상의 모델링 중 비선형 부분의 선형화는 다음과 같이

행하였다. 첫번째는 전류의 제곱에 비례하는 전자기력을 동작점 부근에서 선형화하였고, 두번째는 강체 모델링 시에 센서 위치와 전자석 위치에서의 변위에 관한 비선형 식을 미소 각변위로 간주하여 선형화 하였다. 마지막으로 계측장치에서의 변위와 측정전압 사이의 비선형으로 표현되는 식 또한 동작점 부근에서 선형화하였다.

그리고, 구해진 각각의 모델에 대해 집중제어형 PD 제어, LQR 제어 및 $\mathcal{H}_\infty$ 제어 이론을 이용하여 제어 시스템을 설계하고 각 제어시스템에 대해 응답 시뮬레이션을 행한다. 또한 제어 성능의 비교를 위하여 PD 제어 시스템에 대해서는 DSP 를 이용하여 제어 시스템을 구현하여 응답 실험을 행하였다. 그리고, 제작사가 설계하여 장착한 제어 시스템(진·지상 보상기)에 의한 응답 실험 결과와 비교하였다. LQR 제어 시스템에서는 전차원 관측기를 이용하여 전 상태를 관측하여 상태 피드백하였다. $\mathcal{H}_\infty$ 제어시스템 설계에 있어서는 저차원화 된 공칭모델과 고차 모델 사이의 곱셈형 모델링 오차에 대해 강인한 제어시스템이 되도록 상보감도함수의 하중행렬을 선정하였고, 제어 시스템의 성능에 관여하는 감도함수의 하중행렬은 시행착오적으로 선정 하였다.

응답실험의 비교로부터 본 연구에서 설계한 집중형 PD 제어시스템에 의한 응답이 제작사에 의한 제어 시스템의 응답보다 양호함을 확인할 수 있었다. 그리고 LQR 제어 및 $\mathcal{H}_\infty$제어에 의한 응답 시뮬레이션 결과로부터 설계된 제어시스템의 응답이 양호함을 확인할 수 있었다.

1 Introduction

1.1 Applications of Active Magnetic Bearings

1.2 Research Topics

1.3 Objects of Contents of This Paper

Active Magnetic Bearing (AMB) is a kind of novel high performance bearing which can suspend the rotor by magnetic force. Its contact-free manner between the rotor and stator results in it being able to operate under much higher speed than conventional rolling element bearings with relatively low power losses, as well as being environmental-friendly technology for AMB system having no wear and no lubrication requirements.

1.1 Applications of Active Magnetic Bearings

Patents associated with passive, active, and hybrid magnetic bearings go back more than 150 years. Today, there are many thousands of commercial and research applications of AMBs. AMB technology has proven itself through long-running operation in a variety of applications. Many potential users still believe the economics to be prohibitive. However, the cost of this technology continues to decrease rather rapidly and to facilitate new applications yearly.

There are more than 260 large turbomachines, such as compressors, turboexpanders and pumps, supported by AMBs that are in operation today. AMBs have been used to support turbomachinery units with capacities that range from a few kilowatts to as high as 29,000 kilowatts and with nominal operating speeds as high as 60,000 rpm according to the information compiled from several bearing manufacturers (S2M, Revolve Magnetic Bearings, Inc., and Federal-Mogul). In addition to the use of AMB technology in the turbomachinery industries, also there are considerable efforts in unique

commercial applications such as machine tools, low speed machines etc. A brief summary is presented to demonstrate where the current proven commercial applications exist as following aspects.

Compressors.

1) Centrifugal compressors, in 1985, the first commercial application was called Ingersoll-Rand, which was a centrifugal compressor supported in AMBs, 10,444 kW for the NOVA natural gas pipeline system [1]. At the time of this writing, NOVA has 34 operational turbomachines supported on AMBs. Alves and Alavi (1996) presented data indicating that the reliability of the AMB system had surpassed that of conventional bearing and lubrication systems [2], and that AMB systems had a 99.9% reliability based on NOVA's experience. Similar reliability/availability numbers have been published in AMB manufacturers' literature [1].

2) Hydrogen process compressor, in addition to benefits associated with the elimination of conventional bearing lubrication systems, was made by some manufacturers to take advantage of capabilities of AMBs. Hope et al. (1998) discuss the use of two types of Active Vibration Control (AVC) on a six-stage hydrogen process compressor operating at 20.6 MPa (3000 psi) [3]. One of the AVC modes is an open-loop rotating magnetic flux that is superimposed on top of the control fluxes. The rotating AVC flux is adaptive and effectively creates a force that is counter to the rotating unbalanced force. The AVC flux

is adaptive and can be applied based on the desired reduction of vibrations at a particular location, either along the machine shaft or on a base plate to reduce transmitted forces. The second AVC mode is a synchronous current reduction approach that makes the rotor revolve about its inertial center, reducing the control effort associated with unbalance to near zero.

Turboexpanders, besides compressors, are one of the leading applications of AMBs today. A turboexpander is used to expand gases in order to cool them while recovering energy from the expansion process. They are analogous in operation to an automotive turbocharger. Turboexpanders are used in the processing and separation of a number of gases, both industrial and natural. In this application, the AMB system results in better efficiency and a reduction in the overall weight and "footprint" of the equipment by eliminating the lubrication system. This reduced size is very beneficial for applications such as offshore oilrig installations. Turboexpanders outfitted with AMB systems cover a power range from 68 to 6300 kW, with nominal speed ranges from 7200 to 60,000 rpm [1].

Pumps. There are several pumps are used as follows.

1) There are more than 50,000 turbomolecular pumps (TMPs) supported in AMBs in the field today according bibliography [4]. TMPs are used to achieve ultra high vacuum environments for the manufacture of semiconductors. Conventional ball bearings have proven inadequate in many

TMP applications because of vacuum contamination due to vapors from the bearing lubricant and short bearing life due to high-speed operation. Some TMPs are designed for corrosive gas and process technologies, and the AMB systems allow for greater operational safety than mechanical bearings.

2) Other types of turbo pumps have also been supported in magnetic bearings[5], [6]. Nelik and Jones (1991) discuss the design of an eight-stage, 680 gpm, 3560 rpm boiler feedwater pump. The development of this pump was cofunded by the Electronic Power Research Institute (EPRI), and as of the last published report in 1994 by Closkey and Jones, the pump had been in reliable service for at least 3 years. In this application, the AMB system allows for the design of a closer tolerance of shaft movement. This allows for the minimization of clearances, resulting in increased efficiency of the impeller ring and shaft sealing systems. Payback on the AMB technology in this unit was expected to be about 1 year because of improved reliability in the nonredundant pump. The payback was based on the actual operating and maintenance history of three similar pumps with conventional bearings over the previous 9 years. Hawkins (1997) discusses a shock analysis for AMB-supported systems to meet U.S. Navy specifications. Hawkins points out that the U.S. Navy has several ongoing programs to develop AMB systems for onboard rotating equipment such as circulation pumps, seawater pumps and turbine generators [7]. The potential also exists for underwater noise cancellation of machinery using AMB technology.

3) A single-stage centrifugal canned motor pump is presented by Allaire et al. (1989) and Imlach et al. (1990). It is a 20 hp, 300 gpm, single-stage centrifugal canned motor pump running at 3600 rpm supported in AMBs. The design of this system is introduced in bibliography [8] and [9]. This type of pump does not require mechanical seals because there is a thin can between the rotating motor assembly and stator, allowing for a hermetically sealed arrangement. These pumps are used in applications where the process fluid is highly toxic or difficult to contain. In this type of pump, conventional bearings must be lubricated by the process fluid. This often results in short bearing life and, ultimately, the shutdown of the pump for bearing maintenance, which can result in a release of emissions. The pump design incorporating a canned magnetic bearing assembly similar to the motor assembly can eliminate the problematic conventional bearing maintenance scenario.

New and unique applications. There are several other new and unique commercial applications of AMB technology that will be mentioned here briefly.

1) AMB supported fan used for gas recirculation. The electric utility industry has used magnetic bearings in another specific application. McCloskey and Jones (1994) discuss a project cofunded by the EPRI that is a large fan used for gas recirculation [10]. This application was selected because of a long history of unavailability in this type of fan, often due directly or indirectly to

dust buildup. As a result of the high weight and low speed of the fan shaft, only the upper quadrants of the AMBs were successfully installed, even with the high unbalance load requirements.

2) AMB supported machine tools. For example, several high-speed grinding and high-speed milling machines are in use today. Brunet and Wagner (1994) discuss a 60,000 rpm AMB electrospindle used in the process of creep feed grinding [11]. The process involves very high speed grinding (300 m/s), and the AMB enables the high speed while enabling additional advantages associated with rotor position control. Research is under way to further adapt AMBs to machine tool applications, which will be addressed later in this paper.

3) X-ray tubes are another example of an AMB supported commercial application. For example, AMBs have been used as mounts for the X-ray tubes in computer-aided tomographic scanners by Turnley and Rapho [12].

4) Additional applications include ultracentrifuges, neutron choppers, and cryogenic pumps operating at a few degrees Kelvin.

1.2 Research Topics

In addition to proven commercial applications, many promising new AMB research topics are under investigation. Some of these topics involve

exploiting the capabilities of magnetic bearings, whereas others focus on new applications of this enabling technology. Examples of some of these research topics that are associated with rotating equipment are presented.

Bearingless motors. One of the most exciting research topics under investigation today is the bearingless motor. In this scenario, the electromagnetic actuator acts concurrently as a support bearing and as a motor. With the proper control scheme to create both levitation and rotation, a bearingless motor can be configed. Okada et al. (1995) discuss the control of a permanent magnet bearingless motor, which demonstrates significant progress both theoretically and experimentally [13]. Okada's design involves an internal permanent magnet and a simple feedback control and uses an approximation in describing the shape of the magnetic flux distribution. Speed limitations exist due to the flux distribution approximation. A more accurate approximation would allow for higher speed operation, but this comes with a more complex control requirement. For the sake of successfully developing commercial applications, the bearingless motor should offer motor manufacturers a reduction in hardware requirements, a reduced package size, and improved efficiency, ultimately resulting in reduced costs for the end user.

Biomedical research. AMB technology is currently being investigated for applications in biomedical scenarios. Two of the most promising applications are for external blood pumps and artificial heart designs for human cardiac

assist devices. As with turbomachinery, the use of AMBs eliminates the problems associated with lubricating conventional bearings. Many conventional blood pump and artificial heart configurations consist of centrifugal pumps supported in rolling element bearings. Often, these bearings are lubricated with the "process fluid" (blood) to eliminate the possibility of lubrication contamination. Blood is a poor lubricant and the ball bearings tend to damage the blood cells, causing clotting problems for patients. Several research groups are investigating the application of AMBs to cardiac assist devices [14]-[16]. As early as 1992, Akamatsu et al. (1992) discussed a magnetically suspended impeller for a blood pump [2]. Allaire, Maslen et al. (1996) and Baloh et al. are developing electromagnetic radial and thrust bearings for a heart pump that is approximately 4 inch in diameter and 1.6 inch long. Ueno et al. (1998) discuss the design of a combined motor-bearing system for a centrifugal blood pump.

Machine tool research. Although already in commercial use, research involving machine tool applications of AMBs continues. Issues associated with increasing the stiffness and force capability of AMB systems and active vibration control for reducing tool chatter are under investigation. Obtaining better control methods for maintaining system stability over a range of cutting processes and for the variation of cutting tools is also an important research topic as presented in bibliography [13], [17], [18]. Rundell et al. (1996) examine a continuous state feedback controller with a sliding mode observer for a linear model of a vertical rotor. The control objective is to reject rotor

vibration while tracking a reference position, which is directly applicable to a low-force grinding spindle scenario. Stephens and Jagadeesh (1996) discuss the use of an AMB-based dynamic absorber for tool chatter control. Brunet and Wagner (1994) discuss applications of AMB grinding spindles with integrated magnetic bearing and spindle drive controls for obtaining very fine surface finishes. The ultimate goal of machine tool research is to develop high-accuracy AMB supported machine spindles with both high cutting speeds and high cutting power.

Aircraft jet engines. The research of AMBs to jet engines results in such benefits as increased shaft speed, reduced weight, reduced fire hazard, and longer maintenance intervals. In addition, AMBs are an enabling technology, facilitating the total reconfiguration of current jet engine designs. Conventional bearings are limited to 150°C operation, but high-temperature AMBs can be placed closer to the combustion chamber. This high-temperature operation, in conjunction with higher bearing speed capability, allows for more compact engine designs. Several research groups have investigated issues associated with the aircraft engine application [19]~[22]. Hibner and Lewis (1991) discuss the feasibility of magnetic bearings in aircraft engine applications. Kelleher and Kondoleon (1997) present the development of a customized heat treatment process for a high-strength ferromagnetic material, Hiperco 50 HS, and the use of ceramic-coated copper wire for this application. Field and Iannello (1998) discuss the development and testing of a prototype bearing system with a fault tolerant control scheme

for a 4000 HP Allison gas turbine engine. Lyons et al. (1994) discuss work that was completed on the design and control of a fault tolerant AMB system for aircraft engines at the General Electric Company. Magnetic bearings are currently the subject of a joint NASA–U.S. Army program with significant emphasis on high-temperature applications for future gas turbine engines. The program includes the development of a 600°C test stand at NASA's Glenn Research Center.

Flywheel energy storage systems. Another research whose existence is facilitated by AMB technology is the flywheel system for energy storage[23]–[27]. AMBs allow for higher surface speeds, with lower power losses, than conventional bearings. Flywheel systems are under development for use as stationary uninterruptible power supplies, in mobile applications such as hybrid electric vehicles, and as replacements for batteries in space-based applications. In some of the space-based equipment, such as satellites, the flywheel may be operated as both an energy storage device and a momentum wheel or control moment gyro for attitude control, resulting in an overall reduction in hardware requirements. Wu et al. (1998) discuss the nonlinear control of magnetic bearings for high-speed flywheels. Allaire, Kasarda et al. (1996) and Kasarda et al. (1998) discuss issues associated with power losses in magnetic bearings. Kirk, Anand et al. (1994) and Ahrens et al. (1994) discuss design issues associated with flywheel energy storage systems.

Miniaturized systems. Additional research of AMBs include micro-motors

and other miniature/micro devices [28]-[30]. Bleuler et al. (1994) discuss 8 mm diameter micro-machined active magnetic bearings that have been rotated up to 3000 rpm. Siegwart et al. (1994) discuss eddy current bearings for micro-structure levitation and positioning. Trumper et al. (1994) discuss a hybrid magnetic/fluid bearing for atomic scale motion control that is designed to ultimately achieve 1 angstrom resolution in a 100 mm cube of accessible travel.

AMB force-sensing capability. The inherent nature of the bearing system as a feedback mechanism allows for it to be used as a load cell to measure static and dynamic loads on shafts. In this scenario, the AMB acts concurrently as a support bearing and noninvasive shaft force sensor. In 1992, Humphris (1992) first investigated the use of the bearing as a sensor for machine diagnostic purposes [31]. Other researchers have addressed using the AMB to measure forces from various components [32]-[37]. Guinzburg and Buse (1994) have used the force measurement capability of AMB to measure forces on industrial pumps. Allaire et al. (1995) and Baun and Flack (1999) are also using AMBs in a laboratory pump for the measurement of forces on the rotor from impellers in order to verify computational fluid dynamic models. Knopf and Nordmann (1998) have used the force measurement capability to measure fluid film bearing characteristics for verification of analytical models used in rotor dynamic analyses. Wagner and Pietruszka (1988) used AMBs in a similar fashion to determine turbomachinery seal characteristics. Kasarda (1999) has addressed the use of the noninvasive force-sensing capability in

manufacturing equipment for real-time information for improving statistical process control schemes in the production of textiles and films.

Miscellaneous research. In addition to the projects discussed, a few more topics are presented briefly. In particular, there are significant research efforts to address different control strategies to enhance AMB performance. A good starting point for examining these topics are the proceedings from the first through sixth International Symposiums on Magnetic Bearings and the September 1996 *IEEE Transactions on Control Systems Technology, Special Issue on Magnetic Bearing Control*, edited by Knospe and Collins (1996). Such topics as the use of gain-scheduled $\mathcal{H}_\infty$ robust controllers (Matsumura et al., 1996) and μ synthesis of flexible rotor-magnetic bearing systems (Nonami and Ito, 1996) are addressed [35], [38]. In addition to research focusing on control issues, there has been work to investigate passive magnetic bearings. Post and Ryutov (1998) present a design using a specialized array of permanent magnets on the stator and Litz wire on the rotor to obtain a passive eddy current stabilized bearing which is in theory inherently stable during rotation [39]. Because the bearing is only stable above a certain rotational speed, the design does not technically fall under the bounds of Earnshaw's theorem and, therefore, does not violate his original tenets.

Backup bearings. Today, one of the major barriers facing designers and users of magnetic bearings is how to manage a spinning rotor if power to the AMBs is lost. When the power goes out, high-speed rotors delevitate and must be

supported by a mechanical backup bearing system. Although the reliability of AMB systems has been reported to be as high as 99.9% by Alves and Alavi (1996), it is still necessary to have some type of mechanical backup bearing to support a spinning rotor during unplanned power failures to ensure the safety of equipment and personnel [2]. These backup systems have been known to fail to perform adequately on occasion. Most current state-of-the-art backup bearings consist of a ball bearing with a gap between the inner race and rotor that is smaller than the bearing actuator gap. Ideally this backup system allows the delevitated rotor to decelerate to zero rotational speed without causing damage. Several researchers have completed work associated with understanding and improving rotor performance in mechanical backup bearings. Kirk, Swanson, Kavarana, Wang et al. (1994), Kirk, Swanson, Kavarana and Wang (1994), Kirk, Swanson et al. (1995), and Kirk et al. (1996) have been able to predict transient rotor response and verify it experimentally with a 400 lb rotor that has been delevitated at speeds as high as 8000 rpm [40]~[43]. Swanson et al. (1996) describe test results and numerical simulations associated with this test apparatus [44]. Ishii and Kirk (1996) present work demonstrating that an optimum range of support damping for backup bearing systems can be determined [45]. In addition to this work, researchers are investigating fault tolerant magnetic bearings that can withstand certain fault conditions and remain in operation (Lyons et al., 1994; Maslen et al., 1998) shown in bibliography [22] and [46].

All commercial applications and researches involving magnetic bearings can

hardly be covered in this review. But a broad sampling has been presented to give the reader some idea of the AMB technology and a springboard for investigating a particular application in more depth.

1.3 Objects and Contents of This Paper

The goal of this dissertation is to develop control design for a multi-input/ multi-output (MIMO) AMB system (MBC500 Magnetic Moment, LLC, USA) to achieve high control performance. This research includes:

1) The system identification and modeling:

Here, the system is identified as three kinds of mathematical model such as rigid model, state space flexible model and flexible reduced nominal model respectively, considering the different open-loop characteristics.

2) Three designed controllers:

The performances of the controlled system including stability, settling time, recover ability, and robustness are improved.

3) Simulation and experimental results:

The efficiencies of the control strategies and validities of the modeling applied to the system are improved.

The dissertation is structured as follows:

In chapter 2, to begin with, a linear modeling is discussed. Because there are some nonlinear parts in this AMB system, therewith, some linear approximation methods are derived to linearize magnetic force, geometry relations, sensor responses and even current amplifiers. The rotor is a complex mechanical system, it not only has rigid body characteristics such as translational and slope motion but also bends as a flexible body. Then, simple modeling with a rigid rotor for PD control, a full state space modeling with a flexible rotor for the state variable feedback (SVFB) control, and a reduced nominal modeling with flexible rotor for robust control are computed and illustrated.

In chapter 3, a centralized PD controller is designed. The rotor is assumed as a rigid body and the designed controller could levitate the rotor in experimental testbed, running on a DSP board. The coupling effect from one end of the rotor lead to a slight amount at the other end requires the controller to consider this effect. The centralized PD control method is derived using the negative feedback of the other side signal to compensate the slope displacement caused by the slope movement. Experimental results show that this control method improves system recovery ability to the equilibratory point of displacement.

Chapter 4 presents a control strategy based on linear quadratic regulator (LQR) methodology. The dynamic model of the rotor levitation system is pointed out, and the SVFB controller is developed using a full-order observer considering that all the states are not available as measurements in the system. LQR determines SVFB gain, which can minimize the performance index.

Chapter 5 deals with robust $\mathcal{H}_\infty$ control. The overall system is assumed as a mixed sensitivity minimization problem. Three weighting functions are derived into the system: a complementary sensitivity weighting function covers the modeling error, and the sensitivity weighting function covers system disturbance such as the sensors' noise or processor's noise, and input error weighting function covers the input errors to the system. Such robustness of the control system as the rejection ability of disturbance and modeling error is guaranteed by $\mathcal{H}_\infty$ control methodology. The efficiency of the control strategy and validities of the modeling are shown by simulation results.

In brief, a study of AMB including rotor dynamic, modeling, identification, and controllers design are developed, the further study has to consider more complex actual situations such as gyroscopic effect and more feedback signal.

2 AMB Modeling

2.1 AMB Technology

2.2 Introduction of Experimental Testbed

2.3 Linearization

2.4 Rigid System Modeling for PD Control

2.5 State Space Modeling of Flexible System for SVFB Control

2.6 Reduced Nominal Modeling of Flexible System for Robust Control

2.7 Summary

2.1 AMB Technology

The author summarizes the relative technologies including load, static and dynamic stiffness, bandwidth, actuator power, rotational speed, size, high temperature technology, losses and precision (see appendix A).

Beside these advantages of AMB, some limitations arise from two reasons, the state of the actual technology in design and material, and from basic physical relations. The further technology will consider with these and develop this way as well as wider business applications.

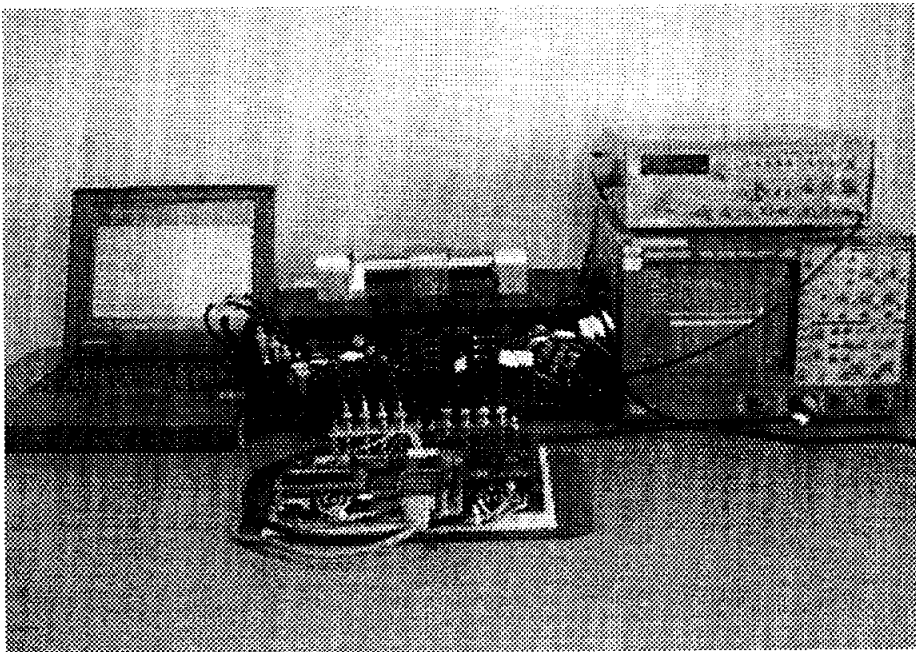## 2.2 Introduction of Experimental Testbed

Fig. 2.1 Experimental Testbed

The bearing system used for this study was the MBC500 from Magnetic Moments, Inc. The MBC500 consists of two sets of active magnetic bearings supporting a complex rotor. The spindle is actively positioned in the radial direction using the integrated analog sensor and control system. The shaft rotates about its longitudinal axis and is driven by an air turbine. To provide a completely selfcontained system, the analog lead controller, sensors and actuators were all integrated into the MBC500. The system accommodated the sensors and actuators as well as bypassing the internal controllers, which made the MBC500 an excellent choice for AMB controller design using other methodologies. In Fig. 2.1, there is a MBC500 in the middle, a DSP board in front of it for outside controller, a PC for programming and an Oscilloscope for monitoring signals.

This system came with its own internal controller that levitated the bearing. In addition, the setup allowed insertion of alternative controllers either in parallel or in replacement of the built-in controller. This proved to be a very useful setup for evaluating a variety of control algorithms. A study started out with the goal of looking at improved control algorithms that could levitate a magnetic bearing more precisely and adjust for changing load conditions on the rotor. This sort of control was envisioned as enabling magnetic bearings to be more suitable for high speed or micro machining applications, where high RPM and very precise control of the rotor location are necessary.

As shown in Fig. 2.2, this system contains a stainless steel rotor which can be levitated using eight "horseshoe" electromagnets, four at each end of the rotor. Hall effect sensors placed just outside of the electromagnets at each end of the rotor measure the rotor end displacement.
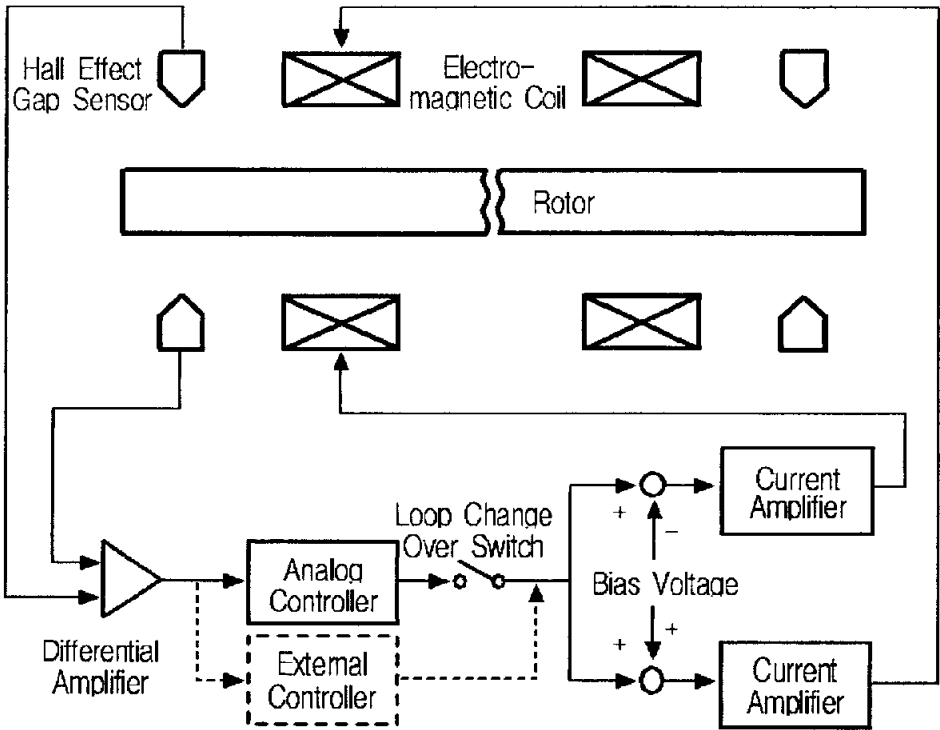
Fig. 2.2 Schematic Diagram of Magnetic Bearing Control System

Fig. 2.3 shows the stereograph and schematic diagram of the rotor. The key papamters of the rotor are shown in Table 2.1.
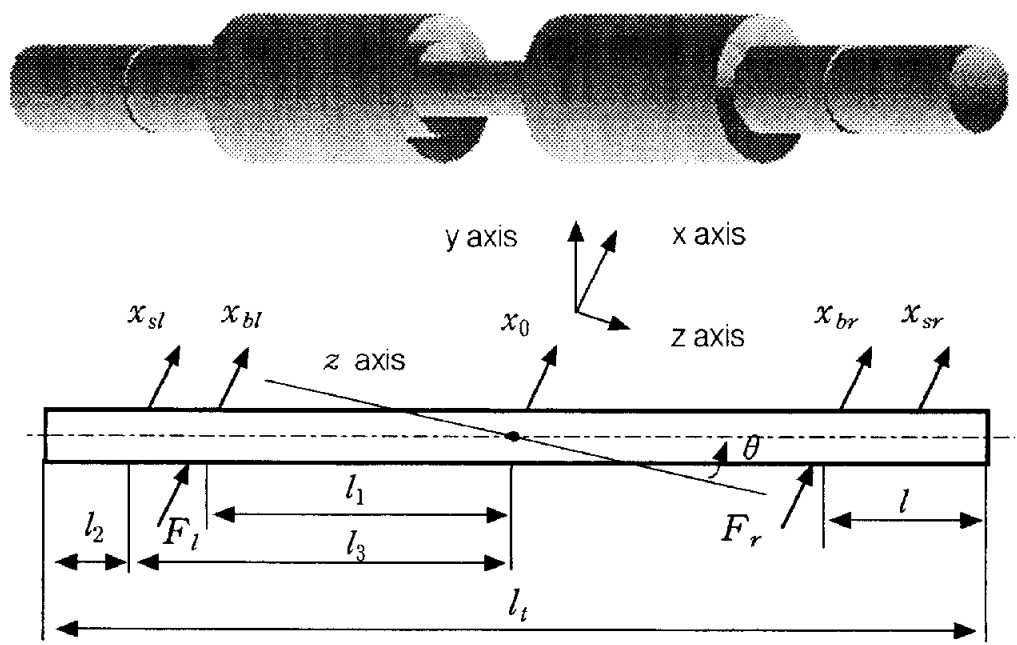
Fig. 2.3 Stereograph and Schematic Diagram of the Rotor

Table 2.1 Key Parameters of Rotor

Symbol	Value
l_t [m]	0.269
l [m]	0.024
l_2 [m]	0.0028
I_0 [kgm^2]	0.0019
m [kg]	0.3073

2.3 Linearization

For the sake of linear control strategy, the author linearized several nonlinear relations in terms of force, geometry, sensors' response and current amplifiers.

2.3.1 Force Linearization

The force exerted by one electromagnet on the rotor is

$$F = \frac{A_s \mu_0 N^2 I^2}{4g^2} \tag{2.1}$$

where A_s is the cross-sectional area of the magnet, μ_0 is the permittivity of free space, g is the gap between the electromagnet and rotor, and N is the number of coil in the magnet, each carrying current I.

Using a Taylor series approximation to linearize the nonlinearity with respect to its two variables about the equilibrium point $(x_i, i_i) = (0, 0)$, yields equation (2.2), and the diagram of force exerted by the eletromagnets versus current and displacement is shown in Fig. 2.4 based on the equation (2.2).

Fig. 2.4 Force Exerted by the Eletromagnets Versus Current and

Displacement

$$\begin{bmatrix} F_l \\ F_r \end{bmatrix} = \begin{bmatrix} R & 0 \\ 0 & R \end{bmatrix} \begin{bmatrix} x_{bl} \\ x_{br} \end{bmatrix} + \begin{bmatrix} S & 0 \\ 0 & S \end{bmatrix} \begin{bmatrix} i_{cl} \\ i_{cr} \end{bmatrix} \tag{2.2}$$

where, R and S is force-displacement coefficient and force-current coefficient respectively (see appendix B).

2.3.2 Geometry Relations Linearization

In rigid model, the displacement at bearing position and sensors position have the relations with x_0 and θ as follows.
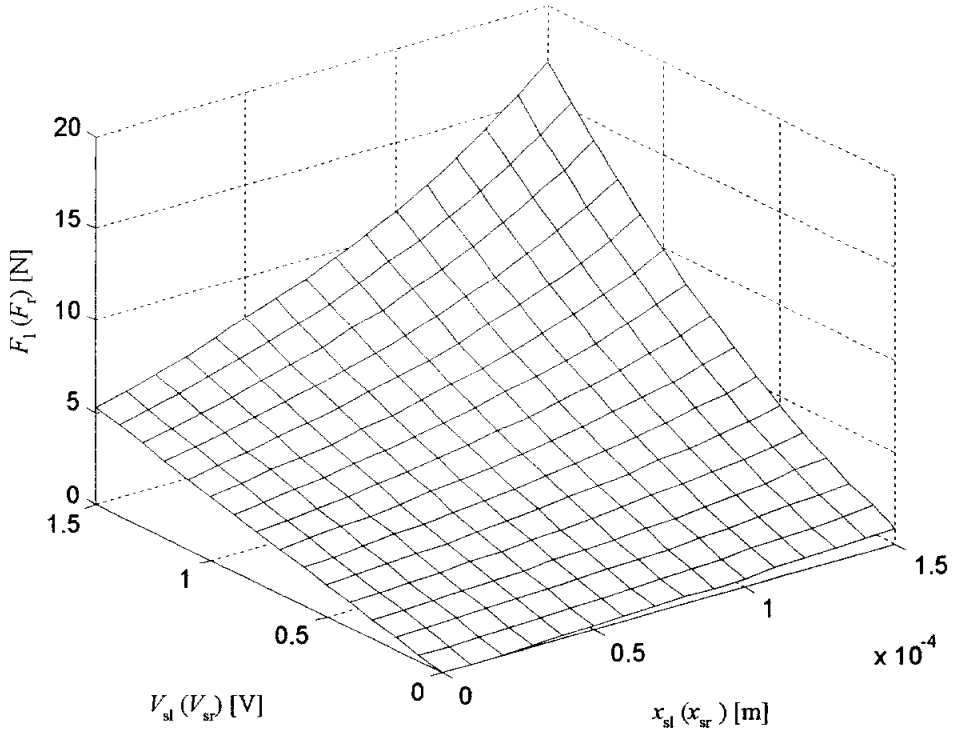
$$\begin{bmatrix} x_{bl} \\ x_{br} \end{bmatrix} = \begin{bmatrix} 1 \\ 1 \end{bmatrix} x_0 + \begin{bmatrix} -(\dfrac{l_t}{2} - l) \\ \dfrac{l_t}{2} - l \end{bmatrix} \sin\theta \qquad (2.3)$$

$$\begin{bmatrix} x_{sl} \\ x_{sr} \end{bmatrix} = \begin{bmatrix} 1 \\ 1 \end{bmatrix} x_0 + \begin{bmatrix} -(\dfrac{l_t}{2} - l_2) \\ \dfrac{l_t}{2} - l_2 \end{bmatrix} \sin\theta \qquad (2.4)$$

where x_0 is the horizontal displacement of the center of mass of the rotor, x_{bl}, x_{br} are the horizontal displacements of the rotor at left and right bearing positions, respectively, x_{sl}, x_{sr} are the horizontal displacements of the rotor at left and right Hall-effect sensor positions respectively, l_t is the total length of the rotor, l is the distance from each bearing to the end of the rotor, l_2 is the distance from each Hall-effect sensor to the end of the rotor, θ is the angle that the long axis of the rotor makes with the z axis.

Fig 2.5 shows the first 2 flexible modes of the rotor, we define the amplitude variables a_1 and a_2 as the amplitude in mode 1 and mode 2 respectively. a_1 and a_2 relate to the rotor displacement at bearing position and sensor position as follows:

$$
\begin{bmatrix} x_{bl} \\ x_{br} \end{bmatrix} = C_{a2b} \begin{bmatrix} a_1 \\ a_2 \end{bmatrix} \tag{2.5}
$$

$$
\begin{bmatrix} x_{sl} \\ x_{sr} \end{bmatrix} = C_{a2s} \begin{bmatrix} a_1 \\ a_2 \end{bmatrix} \tag{2.6}
$$

where, C_{a2b} and C_{a2s} are the dynamic matrix (see appendix B) from the amplitude to the displacement at bearing position and sensor position respectively.

When the θ is small we can approximate $\sin\theta \cong \theta$ and $\cos\theta \cong 1$. Then the relations derived from equation (2.2) and (2.3) are approximated as

$$
\begin{bmatrix} x_{bl} \\ x_{br} \end{bmatrix} = M_{s2b} \begin{bmatrix} x_0 \\ \theta \\ a_1 \\ a_2 \end{bmatrix} \tag{2.7}
$$

$$
\begin{bmatrix} x_{sl} \\ x_{sr} \end{bmatrix} = M_{s2s} \begin{bmatrix} x_0 \\ \theta \\ a_1 \\ a_2 \end{bmatrix} \tag{2.8}
$$

where M_{s2b} and M_{s2s} are dynamic matrix (see appendix B) from the states to the displacement at bearing position and sensor positaion respectively.

Fig. 2.5 Bending Models of Flexible Rotor

2.3.3 Sensor Dynamic Linearization

Considering the sensor non-linearity, we can wirte the relation of the sensor outputs $[V_{sl}\ \ V_{sr}]^T$ and horizontal displacements $[x_{sl}\ \ x_{sr}]^T$ as shown in equation (2.9), and the diagram of sensor voltage output versus displacement is shown in Fig. 2.6 according equation (2.9).

$$\begin{bmatrix} V_{sl} \\ V_{sr} \end{bmatrix} = 5000 \begin{bmatrix} x_{sl} \\ x_{sr} \end{bmatrix} + 0.25 \times 10^9 \begin{bmatrix} x_{sl}^3 \\ x_{sr}^3 \end{bmatrix} \qquad (2.9)$$

By Taylor series approximation, the relation between $[V_{sl} \quad V_{sr}]^{\mathrm{T}}$ and $[x_{sl} \quad x_{sr}]^{\mathrm{T}}$ becomes equation (2.10)

$$\begin{bmatrix} V_{sl} \\ V_{sr} \end{bmatrix} = 5000 \begin{bmatrix} x_{sl} \\ x_{sr} \end{bmatrix} \qquad (2.10)$$
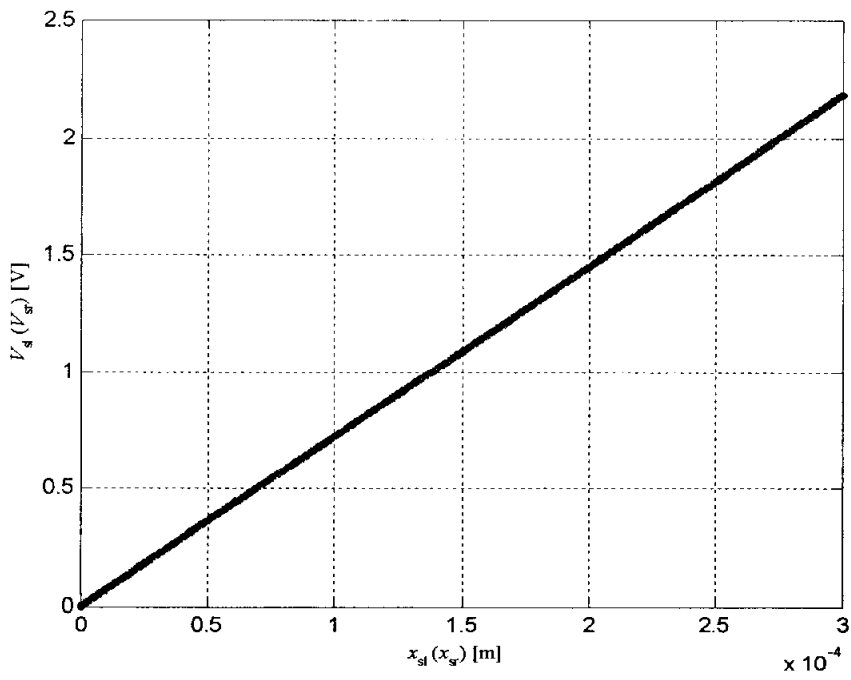
Fig. 2.6 Voltage Output Versus Displacement of Sensor

2.3.4 Current Amplifier Dynamics

There is a current amplifier at the input of the system, that regulates the current into the magnetic coils, which has the following dynamical characteristic between [i_{cl}, i_{cr}] and [$V_{cl} V_{cr}$]:

$$\frac{d}{dt}\begin{bmatrix} i_{cl} \\ i_{cr} \end{bmatrix} = -\frac{1}{2.2 \times 10^{-4}}\begin{bmatrix} i_{cl} \\ i_{cr} \end{bmatrix} + \frac{0.25}{2.2 \times 10^{-4}}\begin{bmatrix} V_{cl} \\ V_{cr} \end{bmatrix} \qquad (2.11)$$

We can simply transfer equation (2.11) to equation (2.12).

$$\begin{bmatrix} I_{cl} \\ I_{cr} \end{bmatrix} = \frac{1}{4}\begin{bmatrix} V_{cl} \\ V_{cr} \end{bmatrix} \qquad (2.12)$$

2.4 Rigid System Modeling for PD Control

As shown in Fig. 2.1, this system contains a stainless steel rotor which can be levitated using eight "horseshoe" electromagnets, four at each end of the rotor. Hall effect sensors placed just outside of the electromagnets at each end of the rotor measure the rotor end displacement.
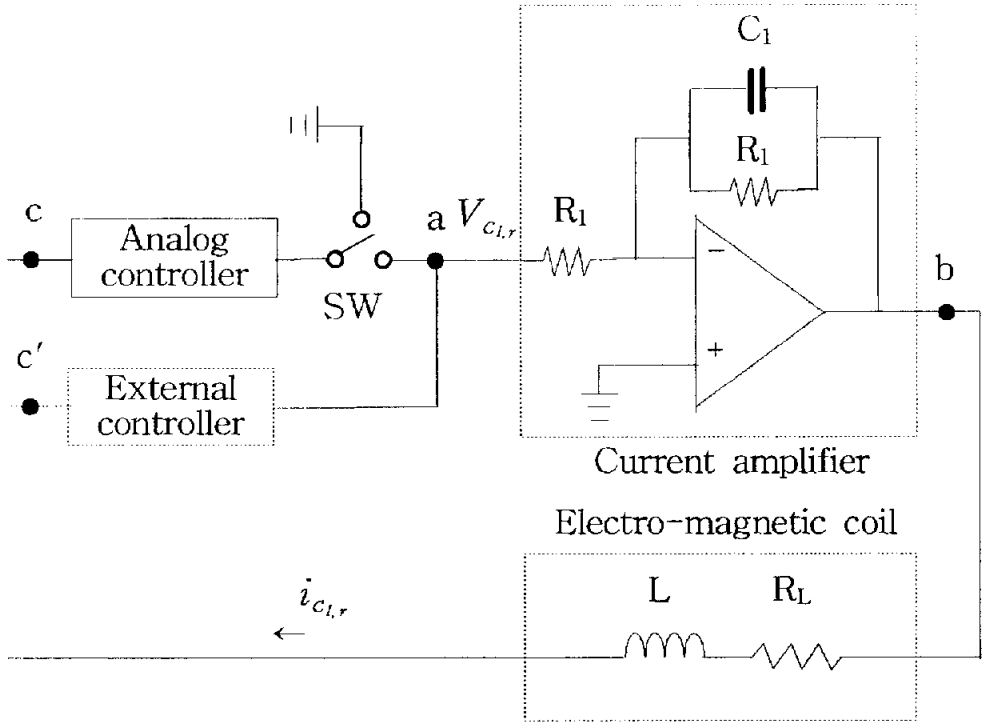
Fig. 2.7 Configuration of Current Amplifier and Electromagnetic Coil

In the AMB system as shown in Fig. 2.2, the rotor as shown in Fig. 2.3 is assumed as a rigid body. In the current amplifier and magnetic coil circuit as shown in Fig. 2.7, we considered the DC gain is 1 from point a to point b, and ignored the effect of the inductance, then the overall state space equation becomes to equation (2.13) [47].

$$\frac{d}{dt}\begin{bmatrix} x_0 \\ \dot{x}_0 \\ \theta \\ \dot{\theta} \end{bmatrix} = \begin{bmatrix} 0 & 1 & 0 & 0 \\ a_1 & 0 & 0 & 0 \\ 0 & 0 & 0 & 1 \\ 0 & 0 & a_2 & 0 \end{bmatrix}\begin{bmatrix} x_0 \\ \dot{x}_0 \\ \theta \\ \dot{\theta} \end{bmatrix} + \begin{bmatrix} 0 & 0 \\ \alpha b_1 & \alpha b_1 \\ 0 & 0 \\ -\alpha b_2 & \alpha b_2 \end{bmatrix}\begin{bmatrix} V_{cl} \\ V_{cr} \end{bmatrix} \qquad (2.13)$$

where, $a_1 = 2\dfrac{S}{m}$, $a_2 = 2\dfrac{R}{I_0}l_1^2$ and $\alpha b_1 = \alpha\dfrac{S}{m}$, $\alpha b_2 = \alpha\dfrac{R}{I_0}l_1$, the

parameters of S and R are the force-displacement coefficient and force-current coefficient of bearing respectively, m is the rotor mass, l_1 is the distance from the rotor mass center to the bearing , I_0 is the mass moment of inertia of the shaft for x-axis or y-axis, if ignore the inductance effect of

magnetic coil, $\alpha = \dfrac{1}{R_L}$ then the output equation is as follow:

$$y_r = \begin{bmatrix} V_{sl} \\ V_{sr} \end{bmatrix} = \begin{bmatrix} c_1 & 0 & -c_2 & 0 \\ c_1 & 0 & c_2 & 0 \end{bmatrix}x_r \qquad (2.14)$$

where, $c_1 = \beta_1$, $c_2 = \beta_1 l_3$, β_1 is the coefficient of displacement-voltage relation in the sensor, l_3 is the distance from the rotor mass center to the sensor.

From the equation (2.13) and (2.14), the overall block diagram of the AMB system can be illustrated as shown in Fig. 2.8.
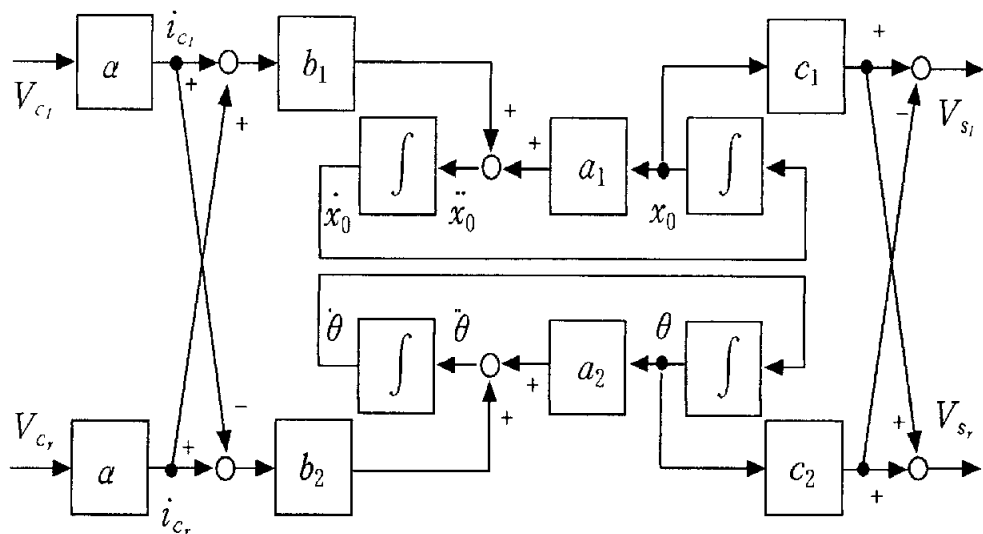
Fig. 2.8 Block diagram of the MB System

From equation (2.13) and (2.14), the previously introduced state space equation and output equation, the overall transfer function matrix is obtained as shown by equation (2.15). Fig. 2.9 is the overall block diagram.

$$G(s) = C(sI - A)^{-1} B = \begin{bmatrix} G_{11} & G_{12} \\ G_{21} & G_{22} \end{bmatrix} \tag{2.15}$$

Where, $G(s)$ is the transfer function matrix of the plant and $G_{11}, G_{12}, G_{21}, G_{22}$ are transfer functions of electromagnets as follow:

$$G_{11} = \frac{(b_1 \alpha c_1 + b_2 \alpha c_2)s^2 - (b_1 \alpha c_1 a_2 + b_2 \alpha c_2 a_1)}{s^4 - (a_1 + a_2)s^2 - a_1 a_2}$$

$$G_{12} = \frac{(b_1 \alpha c_1 - b_2 \alpha c_2)s^2 - (b_1 \alpha c_1 a_2 - b_2 \alpha c_2 a_1)}{s^4 - (a_1 + a_2)s^2 - a_1 a_2} \qquad (2.16)$$

$$G_{22} = G_{11}, G_{21} = G_{12}$$

Through the dynamic experiment of the AMB system and the numerical analysis, the parameters of systems are defined as follow: $a_1 = 58881$, $a_2 = 107588$, $\alpha b_1 = 6.584$, $\alpha b_2 = 114.176$, $c_1 = 10000$, $c_2 = 1308$ and nominal transfer functions are

$$G_{11} = G_{22} = \frac{215186.142s^2 - 15877445495.9119}{s^4 - 166469.0361s^2 + 6334879910.6609}$$

$$G_{12} = G_{21} = \frac{-83497.1788s^2 - 1709258184.5393}{s^4 - 166469.0361s^2 + 6334879910.6609} \qquad (2.17)$$

and the frequency response is as shown in Fig. 2.10[48].
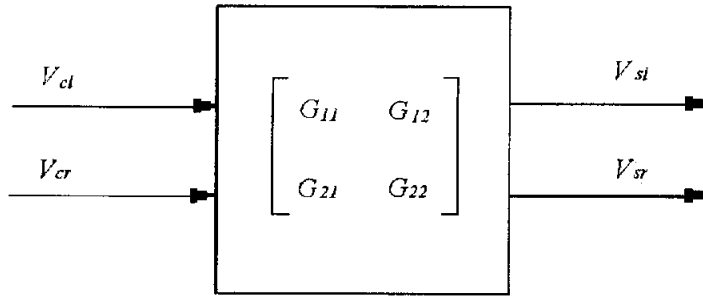
Fig. 2.9 Overall Scheme Block Diagram of Plant
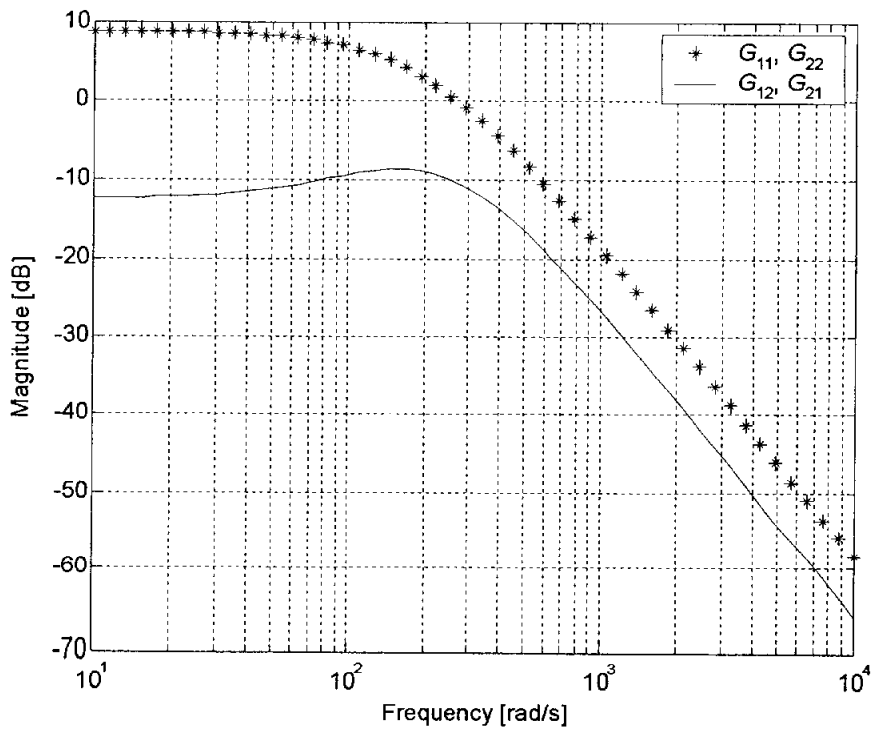
Fig. 2.10 Frequency Response of the Rigid MB System

2.5 State Space Modeling of Flexible System for SVFB Control

Combine all necessary relations in the system such as equation (2.2), (2.7), (2.7), (2.10) and so on, let $[V_{cl} \ V_{cr}]^T$ be the input u and $[V_{sl} \ V_{sr}]^T$ be the output y, $\begin{bmatrix} x_0 & \dot{x}_0 & \theta & \dot{\theta} & a_1 & \dot{a}_1 & a_2 & \dot{a}_2 & i_{cl} & i_{cr} \end{bmatrix}^T$ be state vector x, the overall state space equation becomes to equation (2.18).

$$\dot{x} = Ax + Bu$$
$$y = Cx$$

(2.18)

where, the matrix A, B and C are given in appendix B, and the computing process involves 16 complex steps such as multiplying and transfer computation of matrix as show in appendix C.

state vector $\qquad x = \begin{bmatrix} x_0 & \dot{x}_0 & \theta & \dot{\theta} & a_1 & \dot{a}_1 & a_2 & \dot{a}_2 & i_1 & i_2 \end{bmatrix}^T$ $\qquad$ (2.19)

control input $\qquad u = \begin{bmatrix} V_{cl} & V_{cr} \end{bmatrix}^T$ $\qquad\qquad\qquad\qquad$ (2.20)

sensor output $\qquad y = \begin{bmatrix} V_{sl} & V_{sr} \end{bmatrix}^T$ $\qquad\qquad\qquad\qquad$ (2.21)

where, x_0 is the horizontal displacement of the center of mass of the rotor, θ is the angle that the long axis of the rotor makes with the z axis, In flexible model, we defined the amplitude variables a_1 and a_2 is the amplitude in flexble model and mode 2 respectively, V_{cl} and V_{cr} is control input on left and right side of rotor respectively, V_{sl} and V_{sr} is control output on left and

right side of sensor respectively. The frequency response of the plant is as shown in Fig. 2.11.

2.6 Reduced Nominal Modeling of Flexible System for $\mathcal{H}_\infty$ Control

Derive the state matrix, input matrix and output matrix of the equation (2.18) into equation (2.15), yields the transfer functions matrix of G_{11}, G_{12}, G_{21} and G_{22} as shown in equation (2.22).
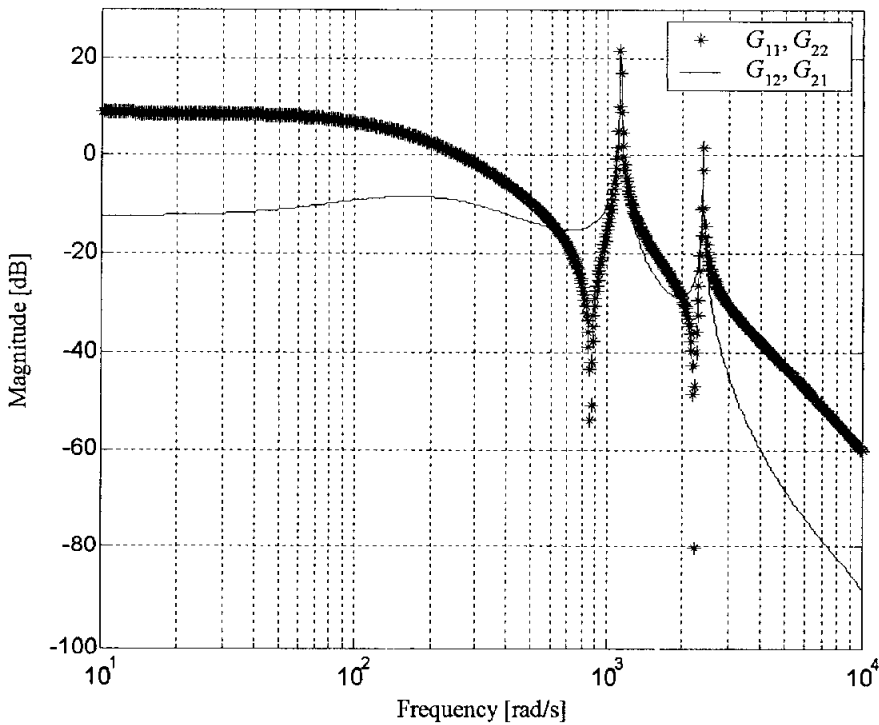
Fig. 2.11 Frequency Response of the Flexible Plant

$$G_{11} = G_{22} = \frac{N_{G11}}{D_{G11}}$$

(2.22)

$$G_{12} = G_{21} = \frac{N_{G12}}{D_{G12}}$$

where,

N_{G11}=$9.0949 \times 10^{-12} s^9 + 4.7684 \times 10^{-7} s^8 + 511011660.5171 s^7 +$
$2.322780 \times 10^{12} s^6 + 7.969358 \times 10^{16} s^5 + 3.622435 \times 10^{20} s^4 +$
$9.651466 \times 10^{23} s^3 + 4.387030 \times 10^{27} s^2 - 4.198334 \times 10^{28} s -$
1.908334×10^{32}

D_{G11}=$s^{10} + 9090.9091 s^9 + 211894128.2637 s^8 +$
$1738481556717.76 s^7 + 7.688554 \times 10^{15} s^6 +$
$3.397691 \times 10^{19} s^5 + 7.684268 \times 10^{22} s^4 - 3.432399 \times 10^{24} s^3 -$
$7.792478 \times 10^{27} s^2 + 7.661700 \times 10^{28} s + 1.741296 \times 10^{32}$

N_{G12}=$9.0949 \times 10^{-12} s^9 + 2.9802 e \times 10^{-7} s^8 - 22698477.6638 s^7 -$
$1.031749 \times 10^{11} s^6 + 6.224678 \times 10^{15} s^5 + 2.829399 \times 10^{19} s^4 -$
$4.014322 \times 10^{23} s^3 - 1.824692 \times 10^{27} s^2 + 3.674843 \times 10^{27} s +$
1.670383×10^{31}

D_{G12}=$s^{10} + 9090.9091 s^9 + 211894128.2637 s^8 +$
$1738481556717.76 s^7 + 7.688554 \times 10^{15} s^6 +$
$3.397691 \times 10^{19} s^5 + 7.684268 \times 10^{22} s^4 - 3.432399 \times 10^{24} s^3 -$
$7.792478 \times 10^{27} s^2 + 7.661700 \times 10^{28} s + 1.741296 \times 10^{32}$

During levitation, there are an infinite number of modes excited in the rotor dynamics, however we will only attempt to model the first 4 modes in lowest frequency. The bending shapes of these modes are described in Fig. 2.12.
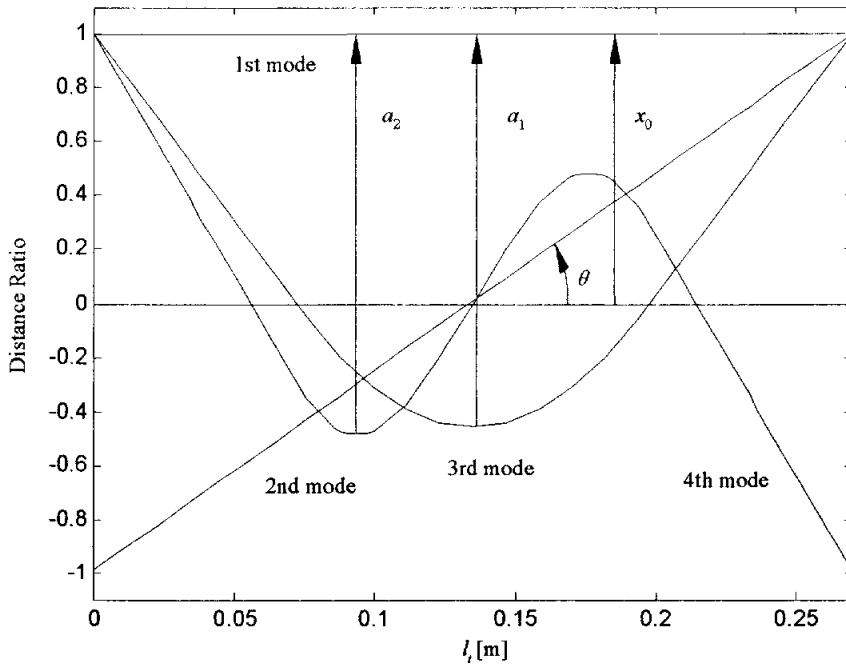
Fig. 2.12 First Four Mode Shapes of the Rotor

During the modeling, it is usually impossible to obtain an exact mathematical model of the plant. Even so, in many instances this model turns out to be unreasonably complex to use for mathematical manipulations in control system design. Thus, the control engineer ends up doing the design for a simpler nominal model whose behavior is representative of the behavior of the actual system. Therefore, for the design made for a nominal plant to work,

one usually asks for the desired properties to be satisfied not only for that particular nominal model, but also for a family of systems, which exist in the uncertainty region around the nominal model. The necessity to work with nominal models, instead of the actual ones motivates the idea of robust control. The $\mathcal{H}_\infty$ theory is a very important tool in robust control, since it offers a natural framework to account for some uncertainty structures during the design stage in order to assure a certain degree of robustness. The uncertainty structure is usually described in the frequency domain that can be easily coped with.

The 4th mode of the rotor happens at high frequency, above 15,000 rpm, so if we omit it and derive the nominal plant in which the rotor has 3 modes of shapes. Let P denote the nominal plant. Where the relation of the actual plant and the nominal plant can be represented in this form:

$$G = (1 + \Delta_m)P \tag{2.23}$$

Then the transfer functions of the nominal plant are:

$$P_{11} = P_{22} =$$

$$\frac{\begin{array}{l} 922295835.0567s^5 + 4192253795712.49s^4 + 662762716524370s^3 \\ + 3.012558 \times 10^{18} s^2 - 2.659683 \times 10^{19}s - 1.208947 \times 10^{23} \end{array}}{\begin{array}{l} s^8 + 9090.9091s^7 + 21846163.3702s^6 + 10772784958.6495s^5 + 24375204916970s^4 \\ - 985429652535736s^3 + 2.237477 \times 10^{18}s^2 + 1.941503 \times 10^{19}s + 4.412506 \times 10^{22} \end{array}}$$

$$P_{12} = P_{21} =$$

$$\frac{\begin{array}{l} 147454423.9579s^5 + 670247381626.453s^4 - 299757954661741s^3 \\ - 1.362536 \times 10^{18} s^2 + 2.328046 \times 10^{19}s + 1.058203 \times 10^{22} \end{array}}{\begin{array}{l} s^8 + 9090.9091s^7 + 21846163.3702s^6 + 10772784958.6495s^5 + 24375204916970s^4 \\ - 985429652535736s^3 + 2.237477 \times 10^{18}s^2 + 1.941503 \times 10^{19}s + 4.412506 \times 10^{22} \end{array}}$$

$$(2.24)$$

Its frequency responses are as shown in Fig. 2.13.
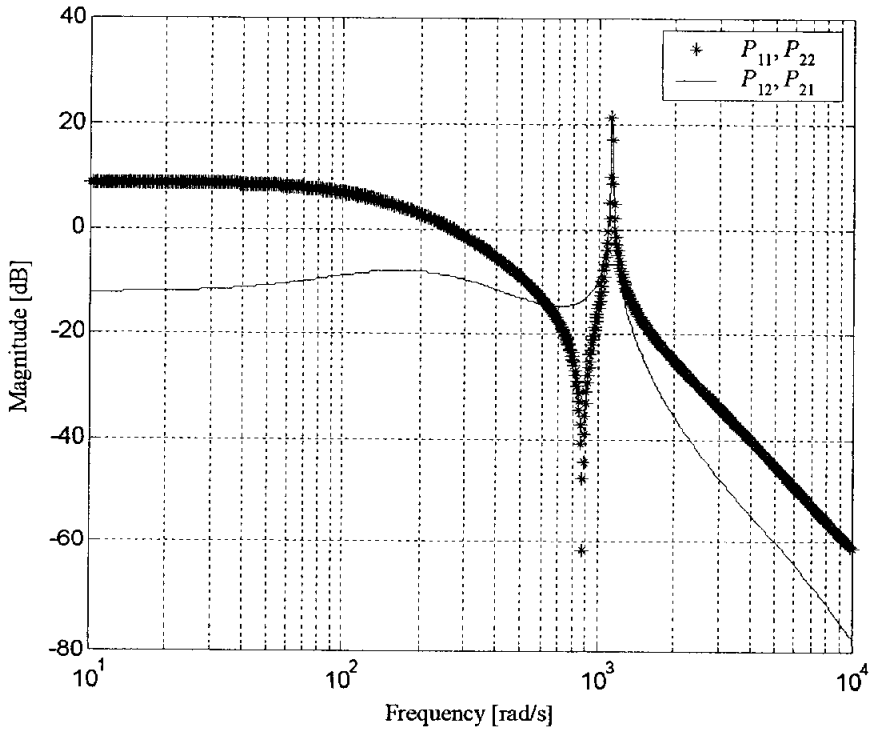
Fig. 2.13 Frequency Response of Nominal Plant
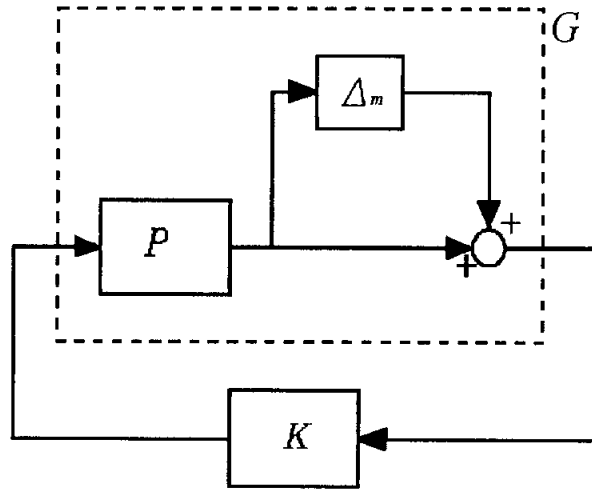
Fig. 2.14 Multiplicative Uncertainty

And the Fig. 2.14 illustrates the uncertainty of the actual plant of the nominal. The multiplicative modeling errors are computed by comparing the plant modeling and nominal plant, they are from two inputs to two outputs respectively, the frequency responses of these modeling errors are shown in Fig. 2.15. For the sake of covering all the errors, the author selected a curve consisted from a set of the greatest value points at each frequency, for example, when lower than 600 rad/s, the errors form $\triangle_{12}$ was selected as overall errors, while from 600 to 1000 rad/s, the errors of $\triangle_{11}$ was selected.
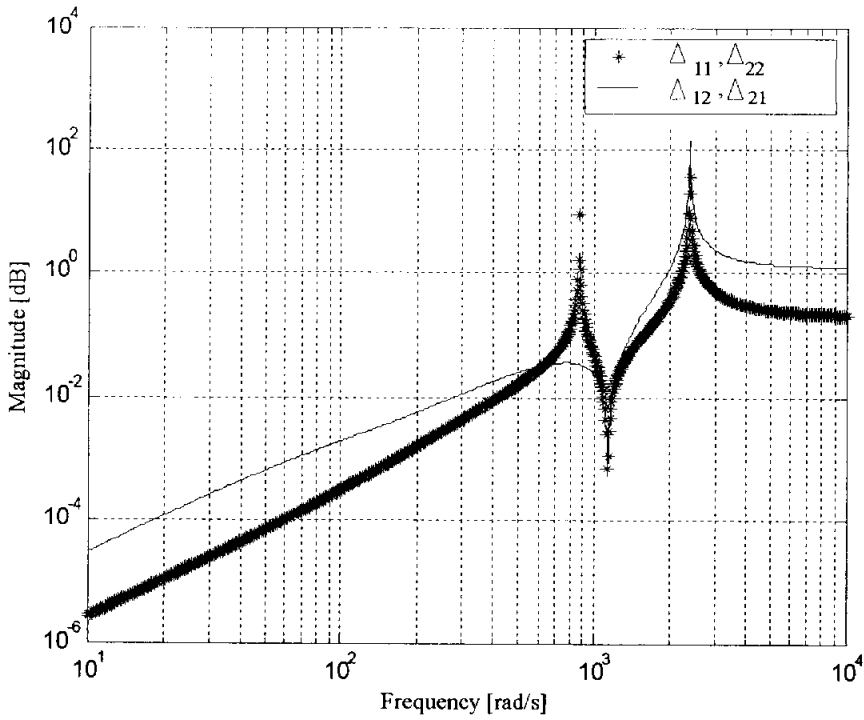
Fig. 2.15 Plot of Plant Uncertainty

2.7 Summary

In this chapter, linear approximation methods are derived to linearize magnetic force, geometry relations, sensor responses and even current amplifiers. A simple modeling with a rigid rotor for PD control, a full state space modeling with a flexible rotor for the state variable feedback (SVFB) control, and a reduced nominal modeling with flexible rotor for robust control are computed and illustrated.

3 PD Control

3.1 PD Controller Design

3.2 Simulation and Experimental Results Analysis

3.3 Summary

3.1 PD Controller Design

In this MIMO AMB rigid rotor system, we assume the rotor is a simple mechanical system, dose not bend but rather experiences only translational or slop motion as a rigid body.

Furthermore, the horizontal rotor is levitated by electromagnets at each end of the rotor. Sensors, outside of the electromagnets, measure displacement at both ends of the rotor. It is hard to ensure the satisfied control performance, if control the rotor at each end independently, because the coupling effect from one end of the rotor lead to a slight amount at the other. So that a controller is demanded to consider this effect to the displacement on its left and right side.

In order to improve the rotor recovery performance to equilibratory point, a suggested control method was introduced compensating rotor slope motion to its principal axis. Then, a digital PD controller was designed and executed on a DSP board[49],[50].

Based on the results of state space equation of the system, a controller is designed to stabilize the levitation for the rigid rotor.

The rotor motion is under the coupling effect from the two sides displacement, without this consideration of the coupling effect, it is hard to get the satisfied

control performance. Therefore, in this part, introduce a method as shown in Fig. 3.5 using the negative feedback of the other side signal to compensate the slope displacement caused by the slop movement, as well as improving recovery ability to the equilibratory point of displacement. That is to say, the controller derives a displacement signal from one side to the other side as the shown in equation (3.1) and (3.2).

$$K_1(s) = K_p(1 + T_d s) \tag{3.1}$$

$$K_2(s) = \lambda K_1(s) \tag{3.2}$$

In this study, $K_1(s)$, as shown in equation (3.1), is a PD controller on the left or right sides and T_d is the differential parameter. While slope displacement is controlled by controller $K_2(s)$ as shown in equation (3.2) and λ is the control voltage proportional to the other side

The background of the suggested control method in this paper is presented in the following part. On principle of the suggested control method, compute equation (2.13) into the form of equation (3.3) and (3.4).

$$m\ddot{x}_0 = k_{mx}x_0 + \kappa_2 \alpha V_{cl} + \kappa_2 \alpha V_{cr} \tag{3.3}$$

$$I_0\ddot{\theta} = k_{mt}xq - \kappa_2 l_1 \alpha V_{cl} + \kappa_2 l_1 \alpha V_{cr} \tag{3.4}$$

where, $k_{mx} = 2k_1$, $k_{mt} = 2\kappa_1 l_1^2$, V_{cl} and V_{cr} are control outputs on left side and right side of the controller separately.

We defined control input vectors of displacement u_x and control input vectors of slop u_t as follow.

$$u_x \equiv \kappa_2 \alpha V_{cl} + \kappa_2 \alpha V_{cr} \qquad (3.5)$$

$$u_t \equiv -\kappa_2 l_1 \alpha V_{cl} + \kappa_2 l_1 \alpha V_{cr} \qquad (3.6)$$

Deriving from equation (3.3), (3.4), (3.5) and (3.6), we can obtain equation (3.7) and (3.8) by which, u_x is considered as the function of x_0, which is the horizontal displacement at the mass center of the rotor, while u_t is considered as the function of θ, which is the slope angle to the axis in counter clockwise.

$$m\ddot{x}_0 - k_{mx} x_0 = u_x \qquad (3.7)$$

$$I_0 \ddot{\theta} - k_{mt} \theta = u_t \qquad (3.8)$$

And equation (3.5) and (3.6) can develop equation (3.9) and (3.10) , that V_{cl} and V_{cr} are the function of u_x and u_t.

$$V_{cl} = \frac{1}{2\kappa_2\alpha}u_x - \frac{1}{2\kappa_2 l_1\alpha}u_t \tag{3.9}$$

$$V_{cr} = \frac{1}{2\kappa_2\alpha}u_x + \frac{1}{2\kappa_2 l_1\alpha}u_t \tag{3.10}$$

Equation (3.11) and (3.12) can be obtained showing the relations between V_{cl}, V_{cr}, x_0 and θ, by substituting equation (3.7) and (3.8) into equation (3.9) and (3.10).

$$V_{cl} = \frac{1}{2\kappa_2\alpha}(m\ddot{x}_0 - k_{mx}x_0) - \frac{1}{2\kappa_2 l_1\alpha}(I_0\ddot{\theta} - k_{mt}\theta) \tag{3.11}$$

$$V_{cr} = \frac{1}{2\kappa_2\alpha}(m\ddot{x}_0 - k_{mx}x_0) + \frac{1}{2\kappa_2 l_1\alpha}(I_0\ddot{\theta} - k_{mt}\theta) \tag{3.12}$$

As control input, u_x and u_t can be denoted as shown by equation (3.13) and (3.14) according to the state feedback control law,

$$u_x = -K_{px}x_0 - K_{dx}\dot{x}_0 \qquad (3.13)$$

$$u_t = -K_{pt}\theta - K_{dt}\dot{\theta} \qquad (3.14)$$

where, displacement parameter, slope parameter, displacement speed gain and slope speed gain are expressed by K_{px}, K_{pt}, K_{dx} and K_{dt} respectively.

Next, combining with equation (3.7), (3.8), (3.13), and (3.14), gives equation (3.15) and (3.16). Based on these two equations we can illustrate the PD control system diagram as shown in Fig. 3.1, and when the reference r_1 and r_2 are zero, block diagram of the overall system becomes Fig. 3.2.

$$\ddot{x} = \frac{k_{mx}}{m}x_0 - \frac{K_{px}}{m}x_0 - \frac{K_{dx}}{m}\dot{x}_0 \qquad (3.15)$$

$$\ddot{\theta} = \frac{k_{mx}}{I_0}\theta - \frac{K_{px}}{I_0}\theta - \frac{K_{dx}}{I_0}\dot{\theta} \qquad (3.16)$$

where,

$$K_{px} = 2\kappa_1\alpha\beta_1(1+\lambda)\ K_p \qquad (3.17)$$

$$K_{dx} = 2\kappa_1\alpha\beta_1(1+\lambda)\ K_pT_d \qquad (3.18)$$

$$K_{pt} = 2\kappa_1\alpha\beta_1(1-\lambda)\ K_p \qquad (3.19)$$

$$K_{dt} = 2\kappa_1\alpha\beta_1(1-\lambda)\ K_pT_d \qquad (3.20)$$
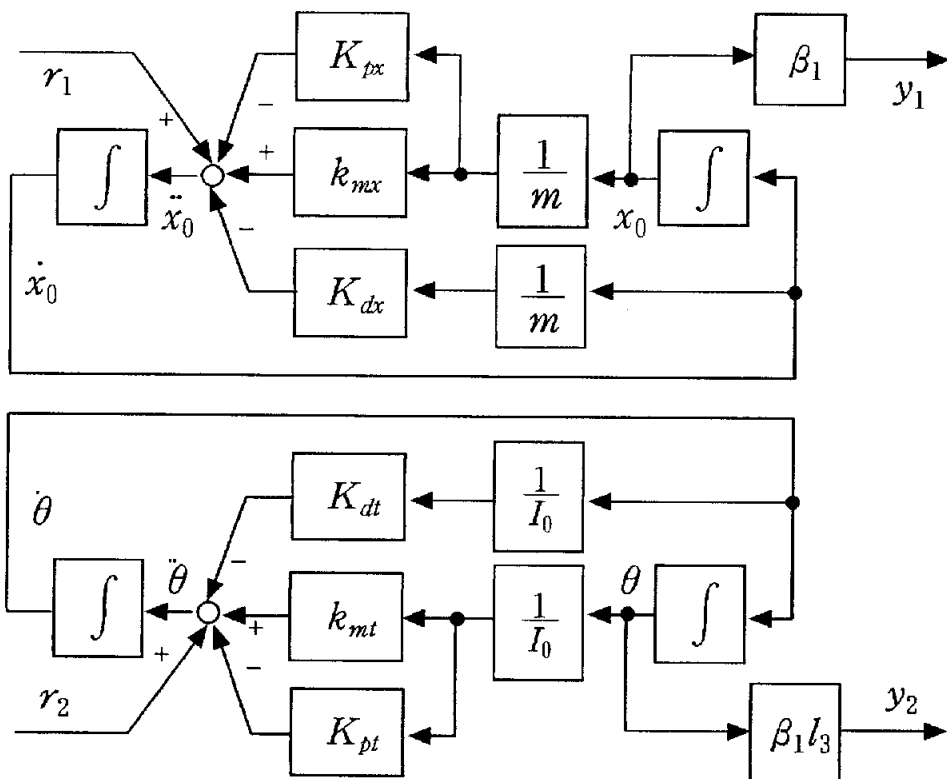
Fig. 3.1 Block Diagram of PD Control System

Using Laplace transformation to equation (3.15) and (3.16), we obtain the characteristics equation as shown by equation (3.21) for this closed loop system. According to Routh-Hurwitz stable criterion for equation (3.21), we can compute the stable condition as shown in inequation (3.22) and (3.23).
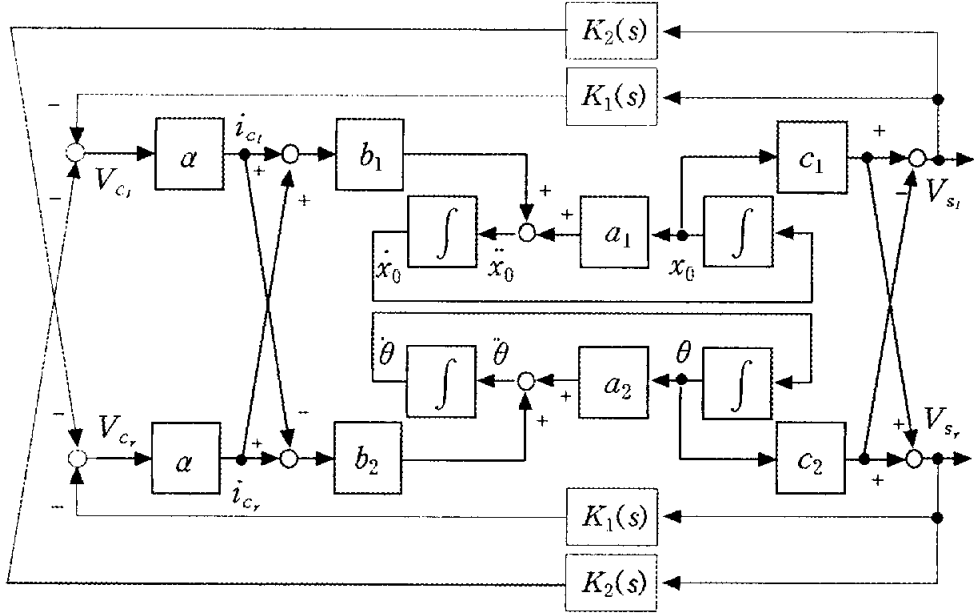
Fig. 3.2 Block Diagram of the Overall System

$$(ms^2 + K_{dx}s + K_{px} - k_{mx})(I_0 s^2 + K_{dt}s + K_{pt} - k_{mt}) = 0 \qquad (3.21)$$

$$K_{dx}(K_{px} - k_{mx}) > 0 \qquad (3.22)$$

$$K_{dt}(K_{pt} - k_{mt}) > 0 \qquad (3.23)$$

In the controlled system with this suggested controller, the transfer functions

of each part of this system are denoted as shown by equation (3.24).

$$G_{11}(s) = \frac{N_{G_{11}}(s)}{D_{G_{11}}(s)}, \quad G_{12}(s) = \frac{N_{G_{12}}(s)}{D_{G_{12}}(s)}$$

$$G_{21}(s) = \frac{N_{G_{21}}(s)}{D_{G_{21}}(s)}, \quad G_{22}(s) = \frac{N_{G_{22}}(s)}{D_{G_{22}}(s)}$$

(3.24)

The transfer functions of controllers are denoted as shown by equation (3.25).

$$K_1(s) = \frac{N_{K_1}(s)}{D_{K_1}(s)}, \quad K_2(s) = \frac{N_{K_2}(s)}{D_{K_2}(s)}$$

(3.25)

Similarly, the equation (3.26) denotes, the closed loop transfer function from r_1 to y_1 and from r_2 to y_1 (see Fig. 3.4).

$$\frac{Y_1(s)}{R_1(s)} = \frac{D_{K_1}(s)\,(N_{G_{11}}(s)N_A(s) - N_B(s)N_{G_{21}}(s))}{N_A(s)N_A(s) - N_B(s)N_B(s)}$$

$$\frac{Y_1(s)}{R_2(s)} = \frac{D_{K_1}(s)\,(N_{G_{12}}(s)N_A(s) - N_B(s)N_{G_{22}}(s))}{N_A(s)N_A(s) - N_B(s)N_B(s)}$$

(3.26)

where,

$$N_A(s) = D_{K_1}(s)D_{G_{12}}(s) + N_{G_{11}}(s)N_{K_1}(s) + N_{G12}(s)N_{K_2}(s)$$

(3.27)

$$N_B(s) = -N_{G_{11}}(s)N_{K_2}(s) - N_{G_{12}}(s)N_{K_2}(s)$$

(3.28)

By using the left and right displacement at points of the bearings x_{bl} and x_{br} as control input, deriving from equation (3.13) and (3.14), yields equation (3.29) and (3.30).

$$u_{xl} = -K_p(1 + T_d s)x_{bl} - \lambda K_p(1 + T_d s)x_{br} \qquad (3.29)$$

$$u_{xr} = -K_p(1 + T_d s)x_{br} - \lambda K_p(1 + T_d s)x_{bl} \qquad (3.30)$$

The roots of the characteristics equation of equation (3.21) were expected at the positions where can let the system is of satisfied settling time and the maximum overshoot critical limit. Such parameters of PD controller as K_p, λ and T_d were tuned by try and error method within the stable bounds given by inequation (3.22) and (3.23). Final amounts were selected as $K_p = 1.2$, $\lambda = 0.4$, $T_d = 0.0002$. The frequency responses of closed loop system is shown in Fig. 3.3.
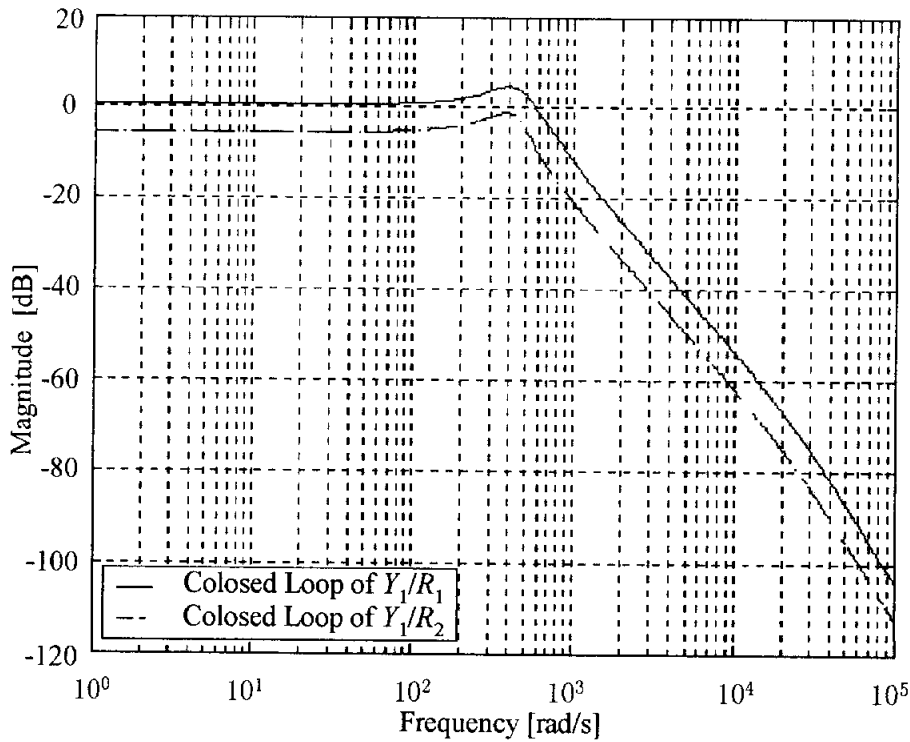
Fig. 3.3 Frequency Responses of Closed Loop System

3.2 Simulation and Experimental Results Analysis

Fig. 3.4 is the time response for the impulse disturbance in the case of control method by using analog lead compensator designed and set on the testbed by a manufacture company. Practically, a ideal impule disturbace cann't achieve, so the impulsion used in the experiment is to stick the rotor by a hammer. Then the outputs of sensor were recored for analysing the responses. While, Fig. 3.5 is the time response for the impulse disturbance in the case of suggested control method by using external digital PD controller.

Fig. 3.4 Time Response to the Impulse Disturbance Using Analog Lead
Compensator

$V_{st} (V_{sr}) $ [V]

2
50 ms
0.50 V

50 ms

1 1 V DC   Time [s]

500 kS/s

2 .5 V DC   1 DC 0.00 V

□ STOPPED
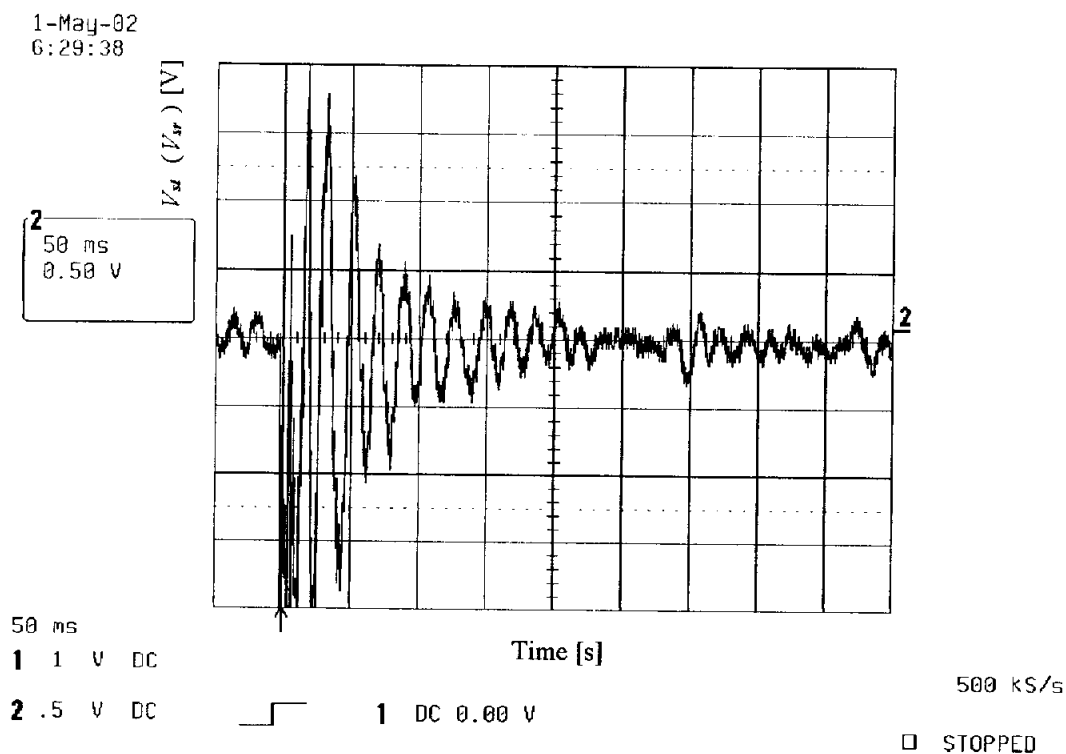
Fig. 3.5 Time Response to the Impulse Disturbance in the Suggested Control
Method Using Digital PD Controller

Also, Fig. 3.6 is the simulation result for the time responses of the impulse
disturbance. In simulation to the controlled system, when the unit impulse
disturbance was acted at the position before the plant, the sensor output was
monitored as the time response.
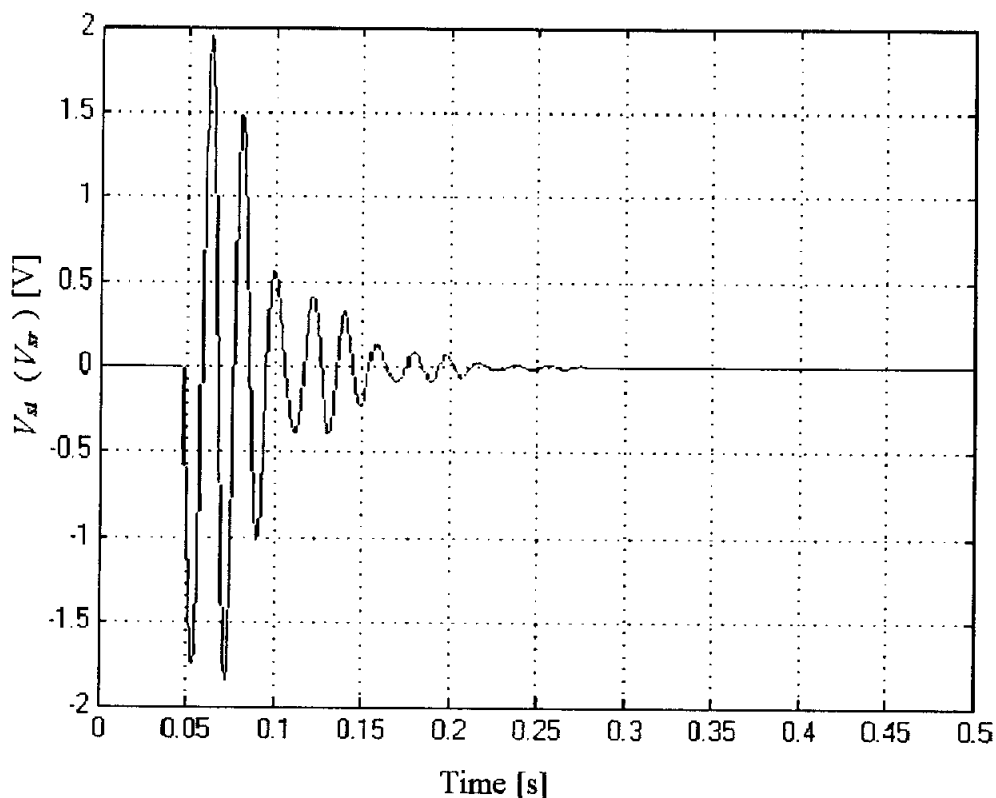
Fig. 3.6 Simulation Time Responses to the Impulse Disturbance for PD
Controller

From the comparison of the results in Fig. 3.4 and Fig. 3.5, we can observe

the control performance clearly. Firstly, the settling time, 500ms in Fig. 3.4,

250ms in Fig. 3.5, it is more quickly to get stable in the later case using PD

controller. Secondly, the steady state error in the later case, 0.05V, is much

smaller than 0.3V in the former case. In other words, this suggested method

using digital PD controller improved the performance dramatically than the lead control method. By comparison Fig. 3.5 to Fig. 3.6, we satisfy that the simulation results well agreed the experiment results, which is identified that the simulation according to the suggested method is correct
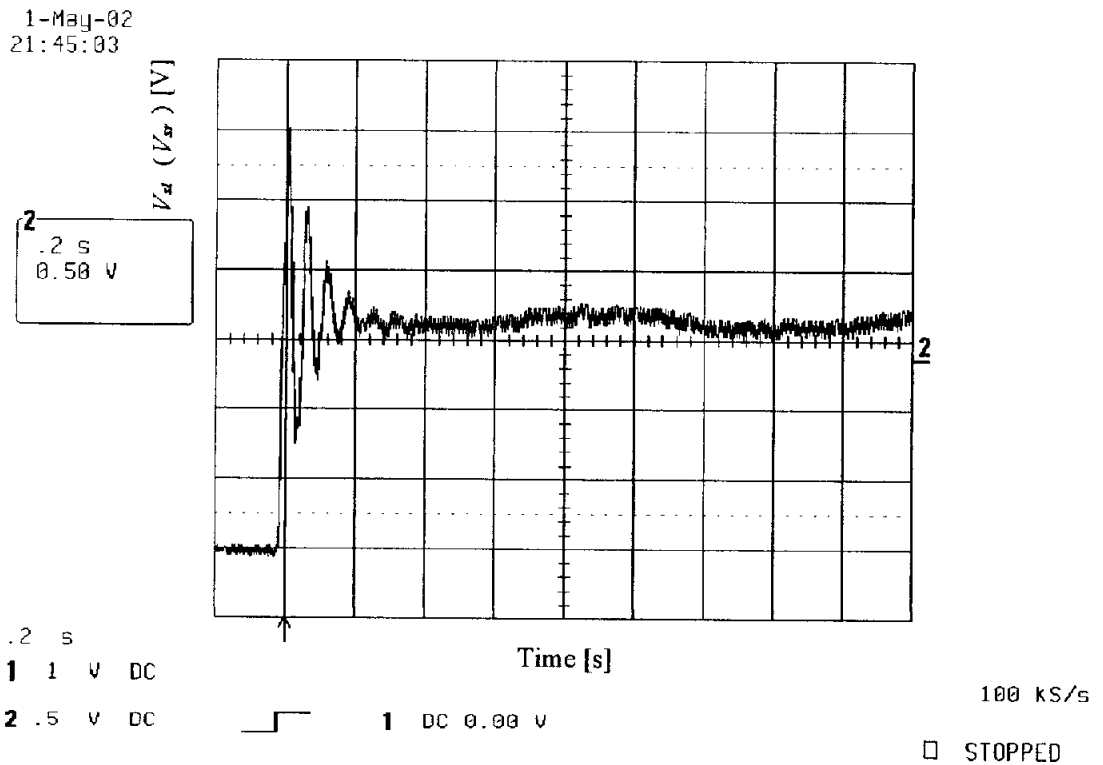
Fig. 3.7 The Response Performance to Step Disturbance in the Control
Method Using Analog Lead Compensator
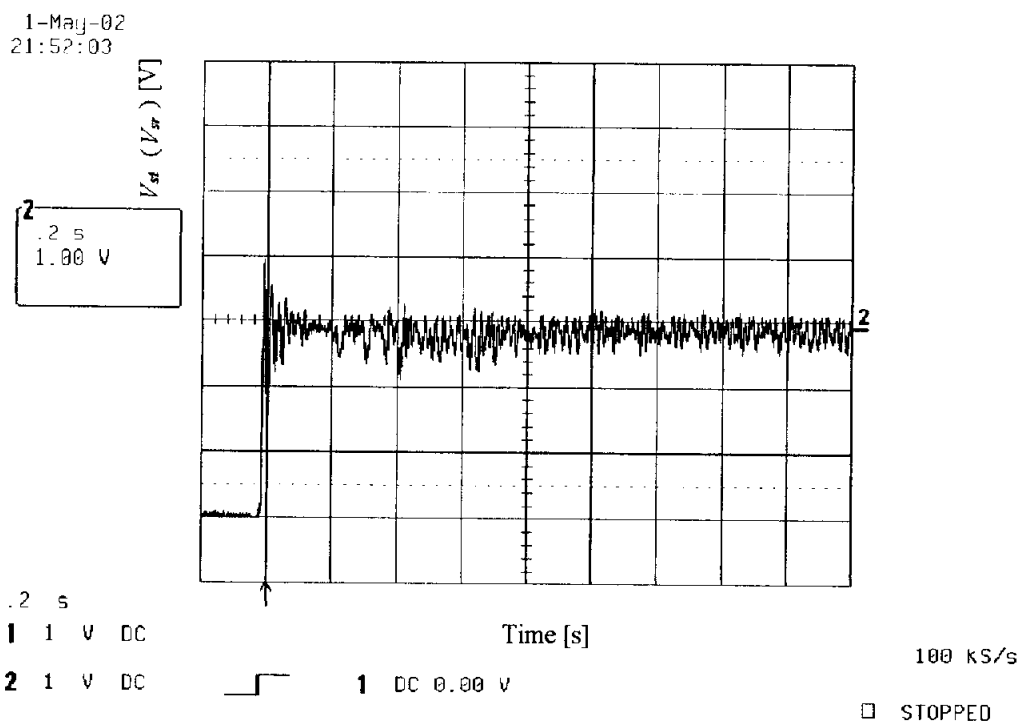
Fig. 3.8 The Response Performance to Step Disturbance in the Suggested
Control Method Using External Digital PD Controller

Fig. 3.7 shows the response performance for the step disturbance in the case
of control method by using analog lead compensator. And Fig. 3.8 is the
response performance for the step disturbance in the case of suggested control
method by using external digital PD controller. While, Fig. 3.9 is the
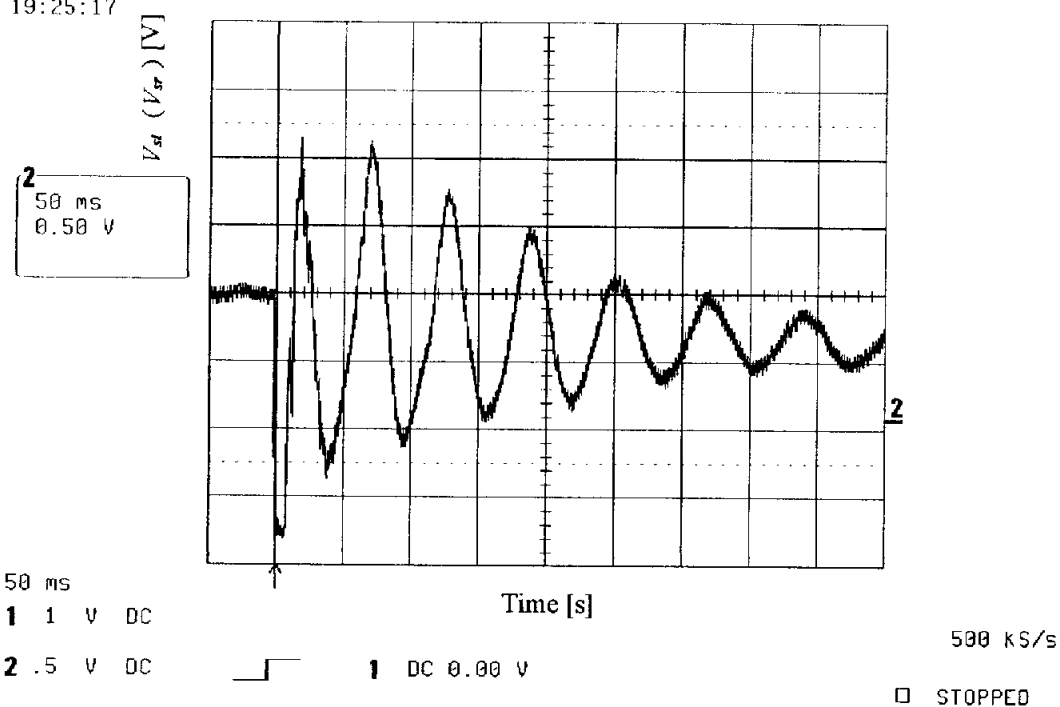simulation result for the time responses of the impulse disturbance.
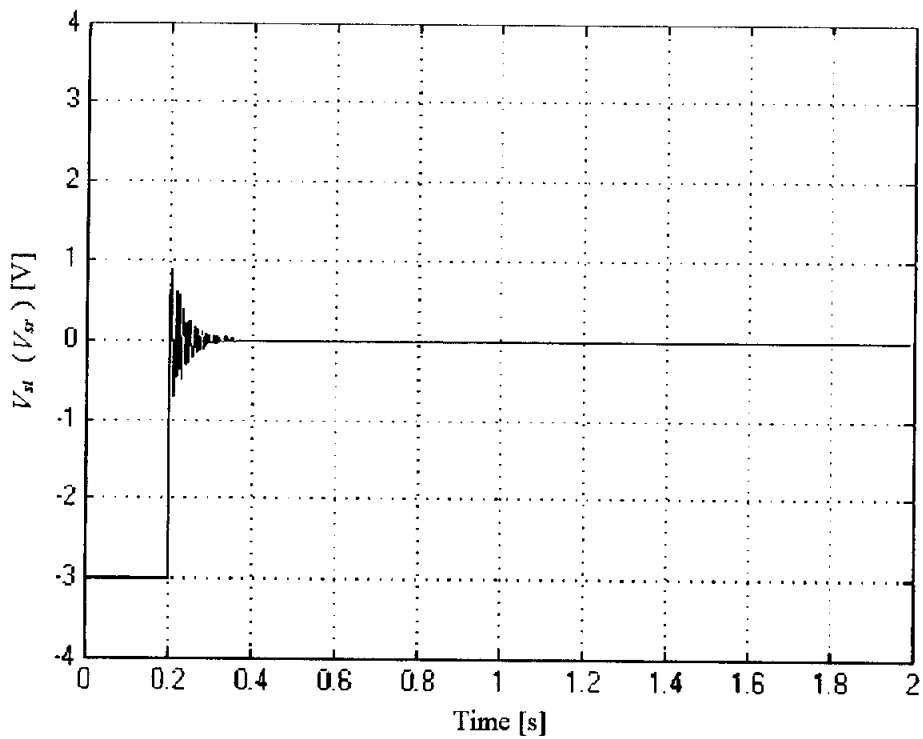
Fig. 3.9 Simulation Response Performance to Step Disturbance for PD
Controller

Similarly, the Fig. 3.7 and Fig. 3.8 show the overshoot are different, it is 1.5V
in Fig. 3.7 and 1V in Fig. 3.8, it is smaller for step disturbance in the case of
using PD control. That is to say, this suggested method improved the
performance. Also, the agreement results of the PD control simulation and
experiment as shown in Fig. 3.8 and Fig. 3.9, identified that the simulation
according to the suggested method is correct again.

Besides, even under the situation of the AMB system being overturned in 360 degree along rotor axis direction or lateral direction, good performance of the AMB system is afforded by this controller.

3.3 Summary

In this chapter, a suggested control method is presented. This method is to derivate a sensor's output signal of the rotor slope from one side to the other side as feedback signal. It can be certified that this suggested method improved the stability and recovery ability from comparison experimental results in terms of the time responses of both impulse disturbance and, step disturbance. The improved performances include settling time, overshoot and steady state error. Using PD controller, the settling time is a half, the overshoot is 67% and the steady state error is 16% as former case using lead control.

The simulations and experiments were in good agreement and showed the method's efficiency and robustness as well as the pertinence of the technological choices made.

4 SVFB Control Strategy

4.1 Full State Feedback Controller Design

4.1.1 Full State Feedback Control

4.1.2 Full Order Observer

4.1.3 Dynamic Regulator Design

4.2 Simulation Results Anlysis

4.3 Summary

4.1 Full State Feedback Control Design

As shown in the state space modeling (see chapter 2.5), there are 10 elements in the state vector (see equation (2.19)), but all the elements are not available to be monitored, so a state variable feedback (SVFB) controller is designed in this chapter to deal with this problem.

4.1.1 Introduction of Full State Feedback Control

The AMB system can be expressed in state variable form as

$$\dot{x} = Ax + Bu$$

(4.1)

with , $x(t) \in R^n$, $u(t) \in R^m$ initial condition is $x(0)$. Assuming that all states are measurable one can easily find a SVFB control

$$u = -Kx + v$$

(4.2)

The closed-loop system using SVFB control becomes

$$\dot{x} = (A - BK)x + Bv = A_c x + Bv$$

(4.3)

with A_c the state space matrix of the closed-loop system and v the new

command input. LQR equation can be used to specify the gain K. We define the performamce index (PI) as

$$J = \frac{1}{2}\int_0^\infty (x^T Qx + u^T Ru)dt \qquad (4.4)$$

substituting the SVFB control into this yeilds

$$J = \frac{1}{2}\int_0^\infty x^T (Q + K^T RK)x dt \qquad (4.5)$$

We assume that input v is equal to zero since our only concern here is the internal stability property of the closed-loop system. Weighting matrices Q, R are user-selected parameters.

The objective in optimal dedign is to find the K that minimize the PI J. It involves solving the following algebraaic Ricatti equation (ARE) for P.

$$A^T P + PA + Q - PBR^{-1}B^T P = 0 \qquad (4.6)$$

then we find the SVFB gain K

$$K = R^{-1}B^T P \qquad (4.7)$$

4.1.2 Full Order Observer

In actual practice, all the states cannot be measured so that SVFB cannot be used. Instead, only a reduced set of measurements given by

$$y = Cx + Du \tag{4.8}$$

is available, where $y(t) \in R^p$.

We build a dynamical system known as full-order observer that can estimate the internal state $x(t)$ given knowledge of the control inputs $u(t)$ and the outputs $y(t)$. This can be accomplished using the scheme shown in the Fig. 4.1.
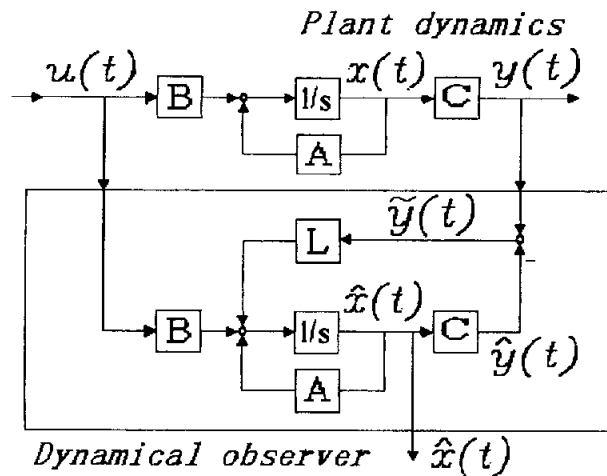
Fig. 4.1 Observer Block Diagram

The equation of the observer is

$$\dot{\hat{x}} = (A - LC)\hat{x} + Bu + Ly \tag{4.9}$$

This is an n-th order dynamical system, with initial state $\hat{x}(0)$ equal to the initial estimate of the state. The observer gain matrix L must be selected so that, even though the initial estimate $\hat{x}(0)$ is not equal to the actual initial state $x(0)$, as time passes the state estimate $\hat{x}(t)$ converges to the actual state $x(t)$.

The quantity $\tilde{y}(t) = y(t) - \hat{y}(t)$ is called the output estimation error. To choose L, define the state estimation error $\tilde{x}(t) = x(t) - \hat{x}(t)$, and write its error dynamics as

$$\dot{\tilde{x}} = (A - LC)\tilde{x} \equiv A_o\tilde{x} \tag{4.10}$$

From this equation, easy to see that as long as we select the observer gain L so that the closed-loop observer matrix

$$A_o = A - LC \tag{4.11}$$

is asymptotically stable, the estimation error $\tilde{x}(t)$ will go to zero asymptotically whatever the initial estimation error

$$\tilde{x}(0) = x(0) - \hat{x}(0) \tag{4.12}$$

To find an observer gain L with desirable characteristics using LQR techniques, simply replace (A, B) by (A^T, C^T) in the LQR design equations to obtain

$$AP_o + P_o A^T + Q_o - P_o C^T R_o^{-1} C P_o = 0 \tag{4.13}$$

$$L = P_o C^T R_o^{-1} \tag{4.14}$$

We have labeled the observer design matrices Q_0, R_0 and the observer auxiliary matrix P_0 with subscripts.

According to The LQR Observer Theorem, the LQR observer under mild conditions is guaranteed to be stable.

4.1.3 Dynamic Regulator Design

Having designed an observer, we now design a feedback controller for the system having output measurements $y(t)$. It can be shown Fig. (3.2) which

provides a dynamic regulator for the plant. The closed-loop system is described by the equations

PLANT $\dot{x} = Ax + Bu$ (4.15)

OBSERVER $\dot{\hat{x}} = (A - LC)\hat{x} + Bu + Ly$ (4.16)

CONTROLLER $u = -K\hat{x} + v$ (4.17)

In general $v=0$. Therefore, the regulator has dynamics provided by the observer, plus a feedback gain portion from the SVFB. The regulator is formally specified by the pair of matrics K and L given in appendix B, other matrics used for computation in this chapter are also given in appendix B.
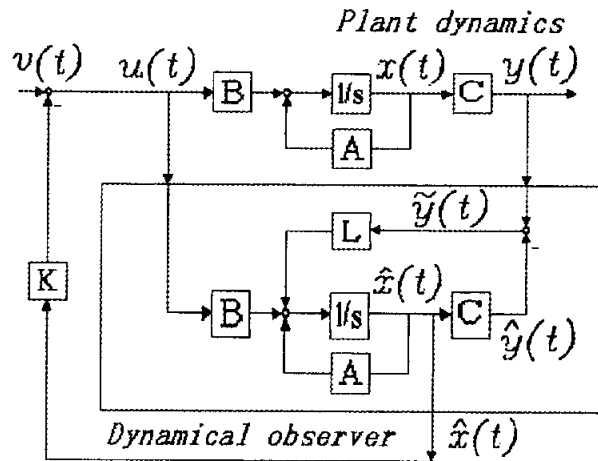
Fig. 4.2 Overall Block Diagram of Plant Observer and Regulator

The proposed regulator only needs the inputs $u(t)$ and the measured outputs $y(t)$, not the full state vector $x(t)$.

The closed-loop dynamics of the overall feedback system are given by

$$\dot{x} = Ax - BK\hat{x} = (A - BK)x + BK\tilde{x} \tag{4.18}$$

$$\dot{\tilde{x}} = (A - LC)\tilde{x} \tag{4.19}$$

Define the augmented system state as $[x, \ \tilde{x}]^{\mathrm{T}}$. Then the closed loop dynamics may be written as

$$\frac{d}{dt}\begin{bmatrix} x \\ \tilde{x} \end{bmatrix} = \begin{bmatrix} A - BK & BK \\ 0 & A - LC \end{bmatrix}\begin{bmatrix} x \\ \tilde{x} \end{bmatrix} \tag{4.20}$$

$$y = \begin{bmatrix} C & 0 \end{bmatrix}\begin{bmatrix} x \\ \tilde{x} \end{bmatrix} \tag{4.21}$$

4.2 Simulation Results Analysis

Fig. 4.3 is the simulation result for the time responses of the impulse disturbance at the same position as output $y(t)$ in Fig. 4.2, and the sensor output was monitored as the time response. The amplitude of the simulation inpulse is 2V, which approaches the sensor output voltage caused by the maximum displacement of the rotor. And the impulsing time is 0.001s.

From the comparison of the results in Fig. 3.7 and Fig. 4.3, we can observe clearly that, firstly, the settling time is 20% shorter through the result shown in Fig. 4.3, secondly, the steady state error in the later case is 0V, in Fig.3.7 it is 0.3V. In other words, this SVFB control strategy improved the performance dramatically than the lead control method.
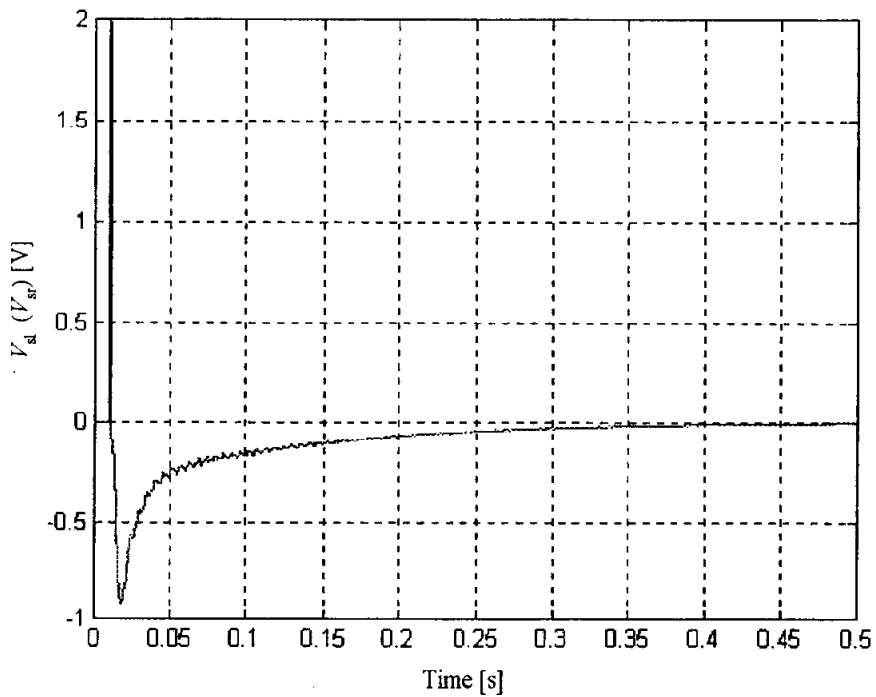
Fig. 4.3 Simulation Response Performance to Impulse Disturbance

4.3 Summary

A SVFB control strategy to MBC500 system is presented. Linear quadratic regulator methodology was derived into the control strategy for the linear plant, the quadratic performance index and the fact that the function of this feedback is to regulate the states to zero. It can be certified performance requirement in case of from simulation results for the time responses of impulse disturbance. We can see that the settling time is 20% shorter and the steady state error is 0V in the disturbance response of this SVFB control system.

On the other hand, there are some disadvantages in the methodology. All the system parameters should be exactly shown because they are the basic hypothesis. However, practically, there is really difficult to exact all parameters such as state space matrix, input matrix and output matrix.

If we can derive them by all means, this method can be efficient in practice.

5 H∞ Control

5.1 Robust Controller Design

5.2 Simulation Results Analysis

5.3 Summary

5.1 Robust Controller Design

Given a nominal plant P, the controller K is required to stabilize not only the nominal plant P, but also all possible real plants G. If we can choose weighting matrix W_T for the bound on uncertainty, necessary and sufficient conditions for robust stabilization are given by

$$\left\| W_T PK(1+PK)^{-1} \right\|_\infty \le 1 \tag{5.1}$$

A typical performance problem is the sensitivity minimization problem. This problem is to find a controller K, which satisfies the equation (5.2). In the equation (5.2) W_S is weighting matrix relating to sensitivity.

$$\left\| W_S (1+PK)^{-1} \right\|_\infty < \gamma \tag{5.2}$$

Generally, the controller is required to satisfy robust performance, i.e., to attain a certain level of performance for all possible plant perturbations. It is hard to find necessary and sufficient conditions for the solvability of the robust performance problem. However, the following constitute simple sufficient conditions for additive and multiplicative uncertainties.

$$\left\| \begin{bmatrix} \gamma^{-1} W_S (1+PK)^{-1} \\ W_T PK (1+PK)^{-1} \end{bmatrix} \right\|_\infty \le 1 \tag{5.3}$$

With solving this optimization problem a robust controller K which stabilized the closed-loop system can be acquired. These problems are sometimes referred to as mixed sensitivity minimization problems. The Fig. 5.1 shows that the weighting function wt that covers the modeling error, and the ws is the sensitivity weighting function that suppresses system disturbance such as the sensors' noise or processor's noise[51],[52].
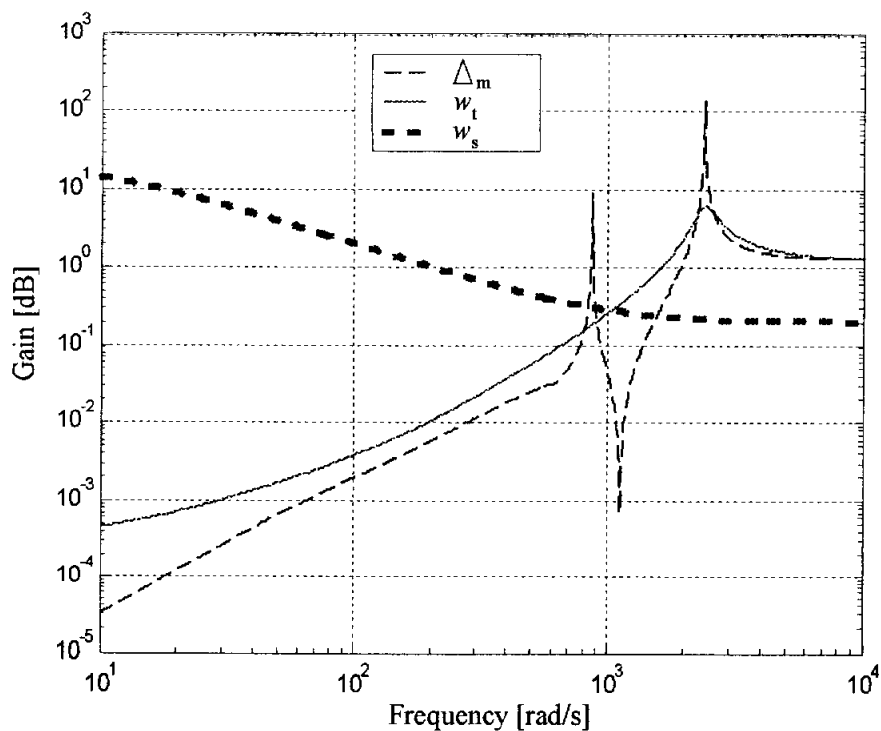
Fig. 5.1 Weighting Functions

The two weighting functions are selected as shown in equation (5.4) and (5.5)

$$w_t = \frac{1.2s^2 + 192s + 1920}{s^2 + 480s + 5760000} \tag{5.4}$$

$$w_s = \frac{0.2s + 200}{s + 10} \tag{5.5}$$

The weighting parameter and weighting functions are chosen as shows in equation (5.5) ~ (5.9). Then the overall system becomes as shown in Fig. 5.2.

$$\gamma = 0.6 \tag{5.6}$$

$$W_T = \begin{bmatrix} w_t & 0 \\ 0 & w_t \end{bmatrix} \tag{5.7}$$

$$W_S = \begin{bmatrix} w_s & 0 \\ 0 & w_s \end{bmatrix} \tag{5.8}$$

$$W_2 = \begin{bmatrix} 0.01 & 0 \\ 0 & 0.01 \end{bmatrix} \tag{5.9}$$
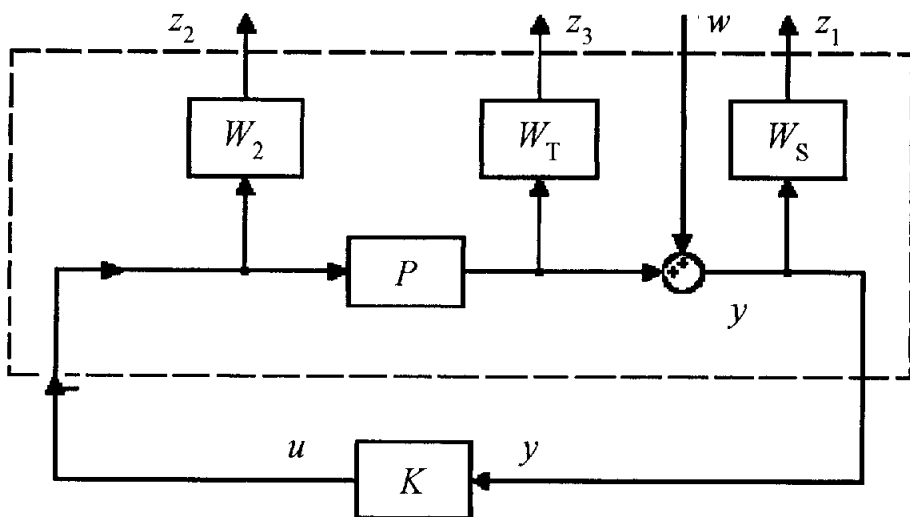
Fig. 5.2 Overall Control System

5.2 Simulation Results Analysis

For the different values of γ, Fig. 5.3 shows the cost function plot that reveals the different energy expenditure on the system. $\gamma = 0.6$ was selected for the $\mathcal{H}_\infty$ controller design.
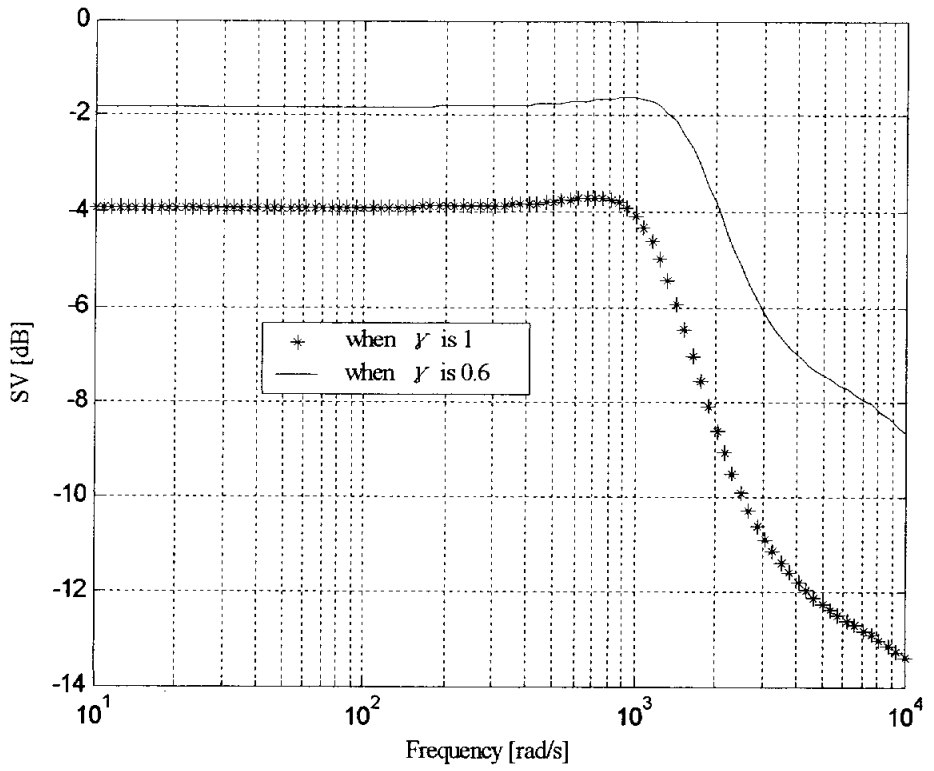
Fig. 5.3 Singular Value Plot of Cost Function
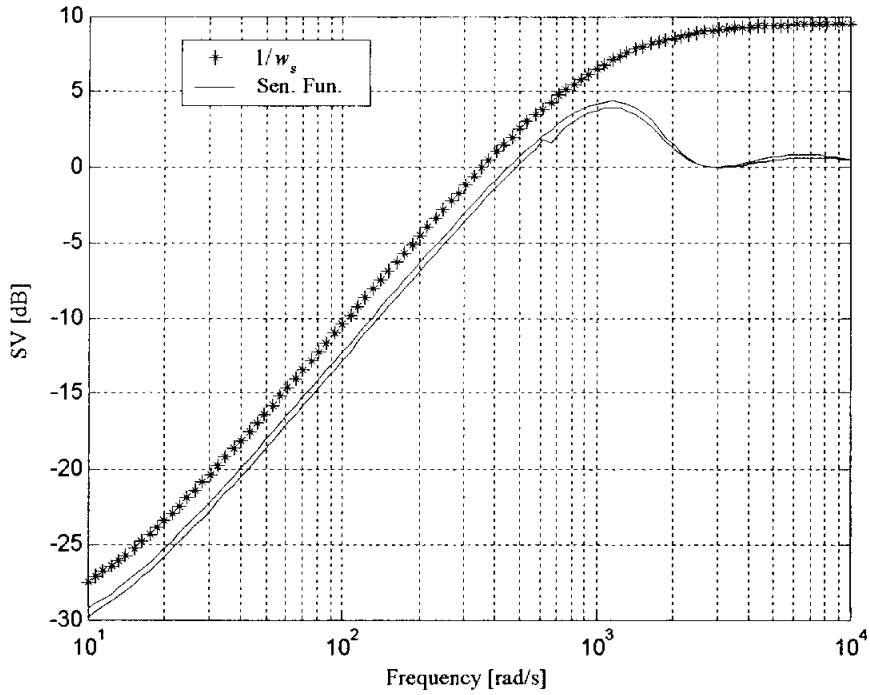
Fig. 5.4 Singular Value Plot of Sensitivity Function

In Fig. 5.4, the singular values of sensitivity functions are under the inverse of sensitivity weighting function. That means the weighting functions can cover its related sensitivity functions, so the controlled system is stable, and the gap between them shows the sensitivity constrain ability is high enough.
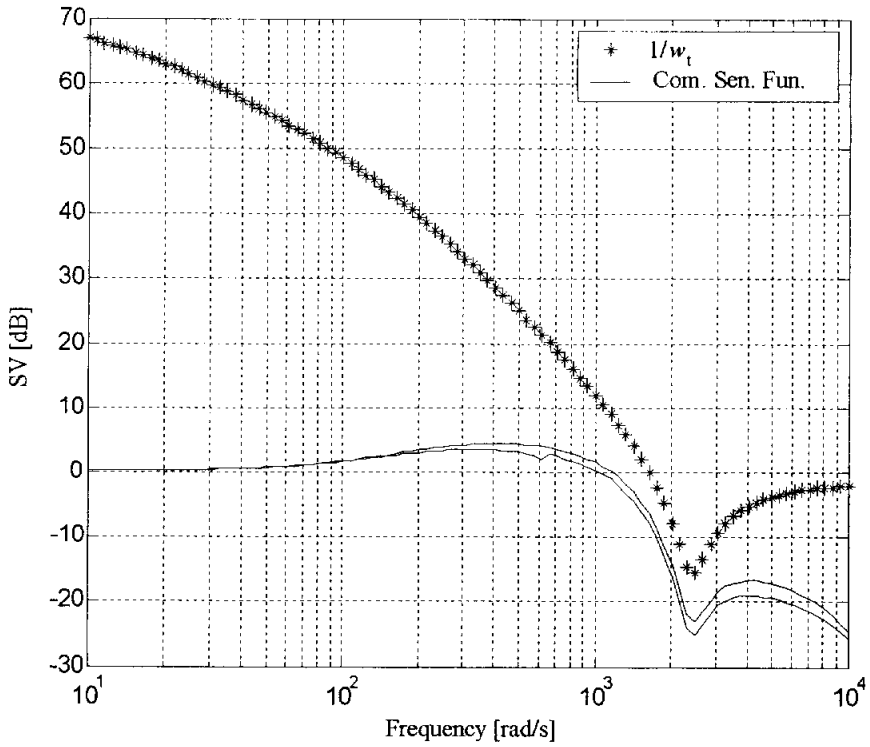
Fig. 5.5 Complementary Sensitivity Function Plot

Similarly, in Fig. 5.5, the singular values of complementary sensitivity functions are under the inverse of complementary sensitivity weighting function. That means the weighting functions can cover its related complementary sensitivity functions, and the system can follow its reference input well.
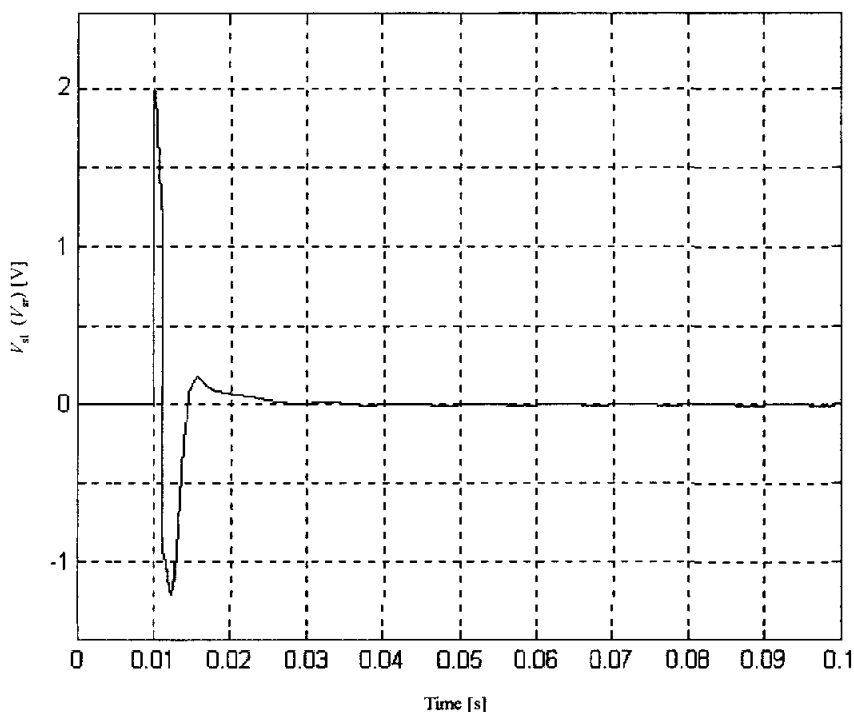
Fig. 5.6 Time Response for the Impulse Disturbance in the $\mathcal{H}_\infty$ Control

Fig. 5.6 is the simulation result for the time response of the impulse disturbance at the position of w as shown in Fig. 5.2, and the sensor output was monitored as the time response. The amplitude of the simulation inpulse is 2V, which is equivalent to the sensor output voltage caused by the maximum displacement of the rotor. And the impulsing time is 0.001s.

From the comparison of the results in Fig. 3.4 with the one of Fig. 5.6, we can observe clearly that, firstly, the settling time, 0.015s, is much shorter in Fig.

5.6, secondly, the steady state error becomes 0 V in Fig. 5.6. In other words, this $\mathcal{H}_\infty$ control strategy improved the performance dramatically than the method using lead compensator.
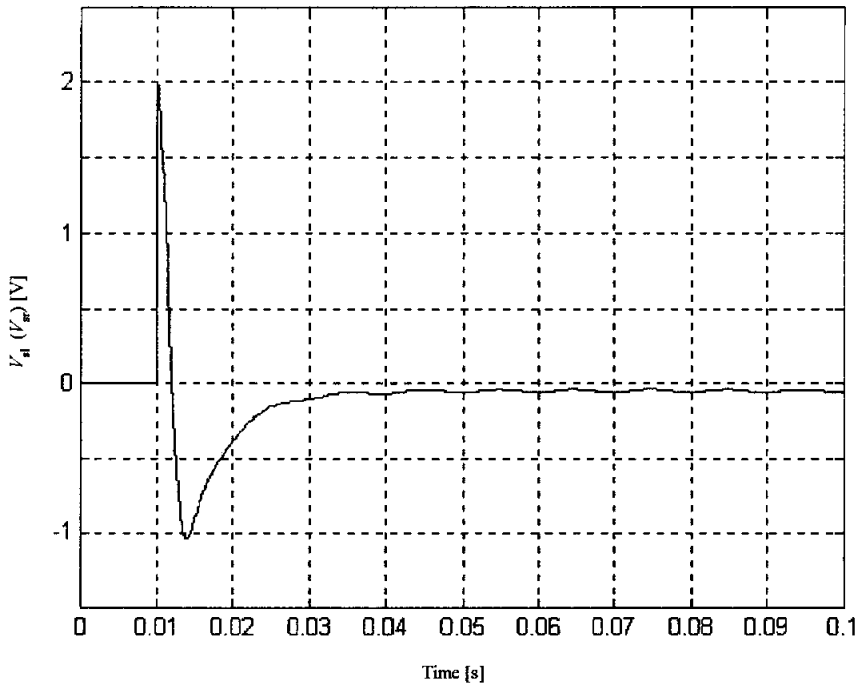
Fig. 5.7 Time Response for the Step Disturbance in the $\mathcal{H}_\infty$ Control

Fig. 5.7 is the simulation result for the time response of the step disturbance at the position of w as shown in Fig. 5.2, and the sensor output was monitored as the time response. The amplitude of simulation inpulse is 2V, which is same value of the sensor output voltage caused by the maximum displacement of the rotor.

The comparison of the results in Fig. 3.7 with the one of Fig. 5.7 shows the settling time, 0.0025s, is much shorter in Fig. 5.7, and there is not overshoot in Fig. 5.7. These reveal that the $\mathcal{H}_\infty$ control strategy improves the performance of the control system dramatically than the method using lead compensator installed in the MBC500 by the manufacture.

5.3 Summary

In this study, a robust control strategy to an electromagetically levitated rotor system was presented. $\mathcal{H}_\infty$ methodology was applied to the control strategy. It can be certified that this method improved the settling, stability and recovery ability from results in terms of the comparison of experiment results with simulation for the time responses of both impulse disturbance and step disturbance. The settling time in the impulse response and step response of $\mathcal{H}_\infty$ Control is the shortest as shown in Fig. 5.8, also the steady state error is the smallest in $\mathcal{H}_\infty$ Control, so $\mathcal{H}_\infty$ Control is the best solution to the MBC500 system.
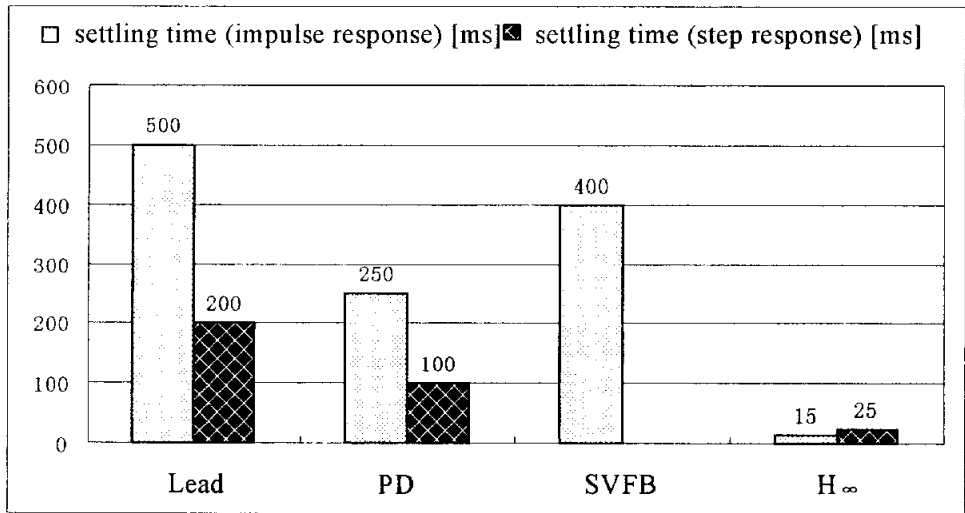
Fig. 5.8 Settling Time in the Impulse Response and Step Response for All the
Control Method in This Study

6 Conclusion

This paper presents the modeling, the identification and the control system design for an AMB system. Through this study, the following results were attained.

In the first place, a suggested control method with respect to centralized PD controller is presented. This method can compensate the opposite displacements, which is caused by slope motion of the rotor. It gives each control signal to the reflection of the each opposite side displacement. It can be certified that this method improved the settling, stability and recovery ability from the comparison of experimental results using lead control, which is installed in the system by the manufacturer LLC, for the time responses of both impulse disturbance and step disturbance. The agreement of the PD experimental results to the simulation results shows that modeling method and the design of controller were well done.

In the second place, a SVFB control strategy, linear quadratic regulator methodology, was introduced in order to design a control system for the MBC500. This methodology can be used to design the control system, only if the all states should be provided, but in most of the controlled systems, it is difficult to derive all states, so in this paper, a full order observer was used to estimate the states. It can be certified that the designed control system regulates the states to zero through the simulations for the time responses of

impulse disturbance. The good simulation performance of this designed control system shows that the SVFB control method can work well on the system and this method is a good alternative to control this system.

In the third place, in $\mathcal{H}_\infty$ control, the MBC500 system was modeled as a reduced nominal model. Theoretically, the modeling error and the disturbance such as the sensor and processor noise are handled by weighting functions, and also the robustness is guaranteed by this methodology. Simulation results of the time responses to both impulse disturbance and step disturbance certified that the settling, stability and recovery ability were improved. It is also shown that the method is efficient and robust and the technological choices are pertinent.

In the fourth place, the author summarized AMB technologies, which are useful to the further study.

At last, further research appears to be indicated in developing insight and outlook at the field of magnetic bearing system. On the one hand, the gyroscopic effects of the rotor and other nonlinear characteristics of the whole system should be considered in order to attain an exact modeling. On the other hand, to instantly derive a feedback signal of rotational speed information will be helpful to achieve more robust performance. More researchers should be involved in the project to deal with this complex work

including rotor dynamics analysis, mathematical modeling, data analysis and computation, DSP programming, experimental realization and so on.

Bibliography

[1] S2M/Actidyne, 1998, Turbomachines Reference List, S2M America, Roanoke, Virginia

[2] Alves, P. S., and Alavi, B. M., 1996, "Magnetic Bearing Improvement Program at NOVA," in International Gas Turbine & Aeroengine Congress and Exhibition, Birmingham, United Kingdom.

[3] Hope, R. W., Tessier, L. P., Knospe, C., and Miyaji, T., 1998, "Adaptive Vibration Control of Industrial Turbomachinery, 98-GT-405," in International Gas Turbine & Aeroengine Congress & Exhibition, Stockholm.

[4] S2M/Actidyne, 1999, Actidyne News (Manufacturer's Publication) No. 9, Sept. 1999, S2M America, Roanoke, Virginia.

[5] Nelik, L., and Jones, G., 1991, "Magnetic Bearings in Boiler Feed Pumps," ROMAG '91: Magnetic Bearings and Dry Gas Seals Conference and Exhibition, Alexandria, Virginia.

[6] McCloskey, T., and Jones, G., 1994, "Magnetic Bearing Projects in the USA Electric Utility Industry," in Fourth International Symposium on Magnetic Bearings, Zurich, 455-462.

[7] Allaire, P. E., Lewis, D. W., and Jain, V. K., 1981, "Feedback Control of a Single Mass Rotor on Rigid Supports," Journal of the Franklin Institute, Vol. 312, 1-11.

[8] Allaire, P. E., Imlach, J., McDonald, J. P., Humphris, R. R., Lewis, D. W., Banerjee, B. B., Blair, B. J., Claydon, J., and Flack, R. D., 1989, "Design, Construction and Test of Magnetic Bearings in an Industrial Canned Motor Pump," in Texas A&M Sixth International Pump Users Symposium, Houston, Texas, 65-73.

[9] Imlach, J., Humphris, R. R., Blair, B. J., Allaire, P. E., and Lewis, D. W., 1990, "Testing of a Magnetic Bearing Equipped Canned Motor Pump for Installation in the Field," in 2nd International Symposium on Magnetic Bearings, Tokyo.

[10] McCloskey, T., and Jones, G., 1994, "Magnetic Bearing Projects in the USA Electric Utility Industry," in Fourth International Symposium on Magnetic Bearings, Zurich, 455-462.

[11] Brunet, M., and Wagner, B., 1994, "Analysis of the Performance of an AMB Spindle in Creep Feed Grinding," in Fourth International Symposium on Magnetic Bearings, Zurich, 519-524.

[12] Turnley and Rapho, 1983, "A Revolutionary Rival That's Challenging the Ball Bearing," BusinessWeek

[13] Rundell, A. E., Drakunov, S. V., and DeCarlo, R. A., 1996, "A Sliding Mode Observer and Controller for Stabilization of Rotational Motion of a Vertical Shaft Magnetic Bearing," IEEE Transactions on Control Systems Technology, Vol. 4, 598-608.

[14] Allaire, P. E., Kasarda, M.E.F., Maslen, E. H., and Gillies, G. T., 1996, "Rotor Power Loss Measurements for Heteropolar and Homopolar

Magnetic Bearings," in Fifth International Conference on Magnetic Bearings, Kanazawa, Japan, 271-276.

[15] Baloh, M. J., Allaire, P. E., Hilton, E. F., Wei, N., Maslen, E. H., Baun, D., Flack, R. D., Olson, D. B., Bearnson, G. B., and Khanwilkar, P. S., 1998, "Magnetic Bearing System for an Artificial Heart," in Sixth International Symposium on Magnetic Bearings, Cambridge, Massachusetts, 77-85.

[16] Ueno, S., Chen, C., Ohishi, T., Matsuda, K., Okada, Y., Taenaka, Y., and Masuzawa, T., 1998, "Design of a Self-Bearing Slice Motor for a Centrifugal Blood Pump," in Sixth International Symposium on Magnetic Bearings, Cambridge, Massachusetts, 143-151.

[17] Stephens, L. S., and Jagadeesh, S., 1996, "Investigation of an AMB Based Auxiliary Mass Dynamic Absorber," in Fifth International Symposium on Magnetic Bearings, Kanazawa, Japan, 423-428.

[18] Wagner, N. G., and Pietruszka, W. D., 1988, "Identification of Rotordynamic Parameters on a Test Stand with Active Magnetic Bearings," First International Symposium on Magnetic Bearings, Zurich, 289-299.

[19] Hibner, D., and Lewis, R., 1991, "Feasibility of Magnetic Bearings for Advanced Gas Turbine Engines," in International Symposium on Magnetic Suspension Technology, Hampton, VA.

[20] Kelleher, W. P., and Kondoleon, A. S., 1997, "A Magnetic Bearing Suspension System for High Temperature Gas Turbine Applications,"

MAG '97: Industrial Conference and Exhibition on Magnetic Bearings, Alexandria, Virginia, 15-24.

[21] Field, R. J., and Iannello, V., 1998, "A Reliable Magnetic Bearing System for Turbomachinery," in Sixth International Symposium on Magnetic Bearings, Cambridge, Massachusetts, 42-51.

[22] Lyons, J. P., Preston, M. A., Gurumoorthy, R., and Szczesny, P. M., 1994, "Design and Control of a Fault-Tolerant Active Magnetic Bearing System for Aircraft Engines," in Fourth International Symposium on Magnetic Bearings, Zurich, 449-454.

[23] Wu, Z. Y., Mellor, P. H., Mason, P. E., and Howe, D., 1998, "Non-Linear Control of Magnetic Bearings for High-Speed Flywheels," in Sixth International Symposium on Magnetic Bearings, Cambridge, Massachusetts, 599-608.

[24] Allaire, P. E., Kasarda, M.E.F., Maslen, E. H., and Gillies, G. T., 1996, "Rotor Power Loss Measurements for Heteropolar and Homopolar Magnetic Bearings," in Fifth International Conference on Magnetic Bearings, Kanazawa, Japan, 271-276.

[25] Kasarda, M.E.F., Allaire, P. E., Norris, P. M., Mastrangelo, C., and Maslen, E. H., 1998, "Experimentally Determined Rotor Power Losses in Homopolar and Heteropolar Magnetic Bearings," Paper No. 98-GT- 317, IGTI/ASME Turbo Expo '98 Conference, Stockholm.

[26] Kirk, R. G., Raju, K.V.S., and Swanson, E. E., 1996, "Evaluation of AMB Turbomachinery Auxiliary Bearings," Colloquium on Turbomachinery, Seoul.

[27] Ahrens, M., Traxler, A., Burg, P. v., and Schweitzer, G., 1994, "Design of a Magnetically Suspended Flywheel Energy Storage Device," in Fourth International Symposium on Magnetic Bearings, Zurich, 553-558.

[28] Bleuler, H., Kawakatsu, H., Tang, W., Hsieh, W., Miu, D., Tai, Y., Moesner, F., and Roner, M., 1994, "Micromachined Active Magnetic Bearings," in Fourth International Symposium on Magnetic Bearings, Zurich, 349-352.

[29] Siegwart, R. Y., Buhler, P., Baumann, D., Neubauer, R. E., 1994, "Eddy Current Bearings for Micro-Structure Levitation," in Fourth International Symposium on Magnetic Bearings, Zurich, 359-363.

[30] Trumper, D. L., Holmes, M., Behrouzjou, R., and Batchelder, D., 1994, "Magnetic/Fluid-Bearing Stage for Atomic-Scale Motion Control," in Fourth International Symposium on Magnetic Bearings, Zurich, 151-155.

[31] Humphris, R. R., 1992, "A Device for Generating Diagnostic Information for Rotating Machinery Using Magnetic Bearings," in MAG '92: Industrial Conference and Exhibition on Magnetic Bearings, Alexandria, Virginia.

[32] Guinzburg, A., and Buse, F. W., 1994, "Axial and Radial Forces on a Pump Impeller Obtained with a Magnetic Bearing Force Measurement

Rig," in Fourth International Symposium on Magnetic Bearings, Zurich, 537-542.

[33] Allaire, P. E., Fittro, R. L., Maslen, E. H., and Wakefield, W. C., 1995, "Measured Force/Current Relations in Solid Magnetic Thrust Bearings," Conference Preprint 95-GT-400, ASME/IGTI Turbo Expo, Houston, Texas.

[34] Baun, D. O., and Flack, R. D., 1999, "A Plexiglas Research Pump with Calibrated Magnetic Bearings/Load Cells for Radial and Axial Hydraulic Force Measurement," Journal of Fluids Engineering, Vol. 121, 126-132.

[35] Knopf, E., and Nordmann, R., 1998, "Active Magnetic Bearings for the Identification of Dynamic Characteristics of Fluid Bearings—Calibration Results," in Sixth International Symposium on Magnetic Bearings, Cambridge, Massachusetts, 52-61.

[36] Wagner, N. G., and Pietruszka, W. D., 1988, "Identification of Rotordynamic Parameters on a Test Stand with Active Magnetic Bearings," First International Symposium on Magnetic Bearings, Zurich, 289-299.

[37] Kasarda, M.E.F., 1999, "Magnetic Bearings for Improved Process Control," in 1999 National Science Foundation (NSF) Grantees Conference, Long Beach, California.

[38] Nonami, K., and Ito, T., 1996, "Mu Synthesis of Flexible Rotor-Magnetic Bearing Systems," IEEE Transactions on Control Systems Technology, Vol. 4, 503-512.

[39] Post, R. F., and Ryutov, D. D., 1998, "Ambient-Temperature Passive Magnetic Bearings: Theory and Design Equations," in Sixth International Symposium on Magnetic Bearings, Cambridge, Massachusetts, 109-122.

[40] Kirk, J. A., Anand, D. K., and Pang, D., 1994, "Performance of a Magnetically Suspended Flywheel Energy Storage System," in Fourth International Symposium on Magnetic Bearings, Zurich, 547-552.

[41] Kirk, R. G., Swanson, E. E., Kavarana, F. H., and Wang, X., 1994, "Rotor Drop Test Stand for AMB Rotating Machinery, Part II: Steady State Analysis and Comparison to Experimental Results," in Fourth International Symposium on Magnetic Bearings, Zurich, Switzerland, pp. 207-212.

[42] Kirk, R. G., Swanson, E. E., Kavarana, F. H., Wang, X., and Keesee, J., 1994, "Rotor Drop Test Stand for AMB Rotating Machinery Part I: Description of Test Stand and Initial Results," in Fourth International Symposium on Magnetic Bearings, Zurich, 202-207.

[43] Kirk, R. G., Swanson, E. E., and Wang, X., 1995, "AMB Rotor Drop Initial Transient on Ball and Solid Bearings," in MAG '95: Industrial Conference and Exhibition on Magnetic Bearings, Alexandria, Virginia, 207-216.

[44] Swanson, E. E., Raju, K.V.S., and Kirk, R. G., 1996, "Test Results and Numerical Simulation of AMB Rotor Drop," IMechE International Conference on Vibrations in Rotating Machinery, Oxford, United Kingdom, 119-132.

[45] Ishii, T., and Kirk, R. G., 1996, "Transient Response Technique Applied to Active Magnetic Bearing Machinery During Rotor Drop," Journal of Vibration and Acoustics, Vol. 118, 154-163.

[46] Maslen, E. H., Sortore, C. K., Williams, R. D., and Aimone, R. J., 1998, "Fault Tolerant Magnetic Bearings," in International Gas Turbine & Aeroengine Congress & Exhibition, Stockholm.

[47] S. H. Shim, C. H. Kim, J. H. Yang, 2001, A study on modeling and identification for the magnetic bearing system, The Korean society for power system engineering Vol.5 No.4, pp.44~52.

[48] S. H. Shim, M. S. Choi, C. H. Kim, 2001, "A   Study on Modeling for the Magnetic Bearing System by Numerical Analysis", The Korean Society for Power System Engineering, Vol. 5, No. 4, pp. 53~60.

[49] S. H. Shim, C. H. Kim, Y. B. Kim, Y. Chang, J. H. Yang (oral), May 10-11, 2003, A Study on Position Control of Magnetic Bearing System by Using DSP, Spring Proceeding of The Korean Society for Power System Engineering, pp. 76~82.

[50] Y. Chang, S. H. Shim, J. H. Yang, 2002, Control Design and Experiment to Levitate a Rotor in an Active Magnetic Bearing System, Journal of the Korean Society for Power System Engineering, Vol. 6, No. 4, pp. 73~80.

[51] Y. Chang, J. H. Yang, 2003, Robust Control System Design for an AMB by H- infinity Controller, Journal of the Korean Society for Power System Engineering. Vol. 7, No. 3, pp. 48~53.

[52] Y. Chang, J. H. Yang, H. H. Jeong, G. H. Choi, Y. W. Kim, (poster), August 25-28, 2003, A Linear Control Strategy Using H-infinity Methodology to an AMB System with a Flexible Rotor, The 32nd International Congress and Exposition on Noise Control Engineering, Seogwipo, Korea, pp.376~382.

[53] Partick Barney, James Lauffer, James Redmond, William Sullivan, February, 2000, "Active control of magnetically levitated spindel" Sandia report , SAND2001-0757, Presented at the International Modal Analysis Conference.

[54] Rundell, A. E., Drakunov, S. V., and DeCarlo, R. A., 1996, "A Sliding Mode Observer and Controller for Stabilization of Rotational Motion of a Vertical Shaft Magnetic Bearing," IEEE Transactions on Control Systems Technology, Vol. 4, 598-608.

[55] Rebecca Petteys, Gordon Parker, James Redmond, 2000, "Disturbance Rejection Control of an Electromagnetic Bearing Spindle" SAND2001-0757, Presented at the ASME International Mechanical Engineering Congress and Exposition, November.

[56] Schweitzer, G., and Lange, R., 1976, "Characteristics of a Magnetic Rotor Bearing for Active Vibration Control," Paper No. C239/76, First International Conference on Vibrations in Rotating Machinery, Institution on Mechanical Engineers, Cambridge, United Kingdom.

[57] Stephens, L. S., and Jagadeesh, S., 1996, "Investigation of an AMB Based Auxiliary Mass Dynamic Absorber," in Fifth International Symposium on Magnetic Bearings, Kanazawa, Japan, 423-428.

[58] Matsumura, F., Namerikawa, T., Hagiwara, K., and Fujita, M., 1996, "Application of Gain Scheduled H-Infinity Robust Controllers to a Magnetic Bearing," IEEE Transactions on Control Systems Technology, Vol. 4, 484-493.

[59] Mark.S. Whorton, August 1997, "High Performance Robust Control of Flexible Space Structures" A Dissertation Presented to The Academic Faculty, In Partial Fulfillment of the Requirements for the Degree Doctor of Philosophy in Aerospace Engineering, Georgia Institute of Technology.

[60] Murat Zeren, , 1997 , "Strong Stabilization and Stable H-Infinitive Controller Design ", Dissertation , Presented In Partial Fulfillment Of The Requirements For The Degree Doctor Of Philosophy In The Graduate School Of The Ohio State University.

[61] Baloh, M. J., Allaire, P. E., Hilton, E. F., Wei, N., Maslen, E. H., Baun, D., Flack, R. D., Olson, D. B., Bearnson, G. B., and Khanwilkar, P. S., 1998, "Magnetic Bearing System for an Artificial Heart," in Sixth International Symposium on Magnetic Bearings, Cambridge, Massachusetts, 77-85.

[62] Brunet, M., and Wagner, B., 1994, "Analysis of the Performance of an AMB Spindle in Creep Feed Grinding," in Fourth International Symposium on Magnetic Bearings, Zurich, 519-524.

[63] Chiba, A., Yoshida, K., and Tadashi, F., 1998, "Transient Response of Revolving Magnetic Field in Induction Type Bearingless Motors with Secondary Resistance Variations," in Sixth International Symposium on Magnetic Bearings, Cambridge, Massachusetts, 461-475.

Appendix A

AMB Technology Summary

Magnetic bearings are increasingly being used for a large variety of applications. Their unique features make them attractive for solving classical rotor-bearing problems in a new way and allow novel design approaches for rotating machinery [53]-[63]. Classical limitations can be overcome and feature ranges can be extended. Of course, limitations still hold, imposed by principally valid physical constraints and by the actual state of the art.

1 Load

The term load already, as simple as it seems, touches upon basic properties of magnetic bearings. The load capacity depends on the arrangement and geometry of the electromagnets, the magnetic properties of the material, of the power electronics, and of the control laws - a set-up with main elements. Furthermore, carrying a load is not just a static behaviour – usually it has strong dynamic requirements. Subsequently, first the static properties of an AMB and the generation of magnetic forces will be briefly outlined .

2 Static and Dynamic Stiffness, Bandwidth, Actuator Power

The stiffness of a bearing characterizes its spring-like behavior, i.e. the ratio

of the supported load with respect to the resulting displacement of that load. The term is based on the understanding that a bearing is a mechanical element. In classical bearings the stiffness stems for example from the elasticity of the oil film or the deformation of balls and inner ring of a ball bearing. In an AMB the force is generated by a control current, which can be adjusted to the needs and opens a novel way of shaping the stiffness and even the overall dynamic behavior, and thus the term "stiffness" may not be the best way to describe the performance of an AMB, but is still used for comparison reasons with classical bearings.

3 Rotational Speed

The features characterizing a high-speed rotor can be looked at under various aspects. The term "high-speed" can refer to the rotational speed, the circumferential speed of the rotor in a bearing, the circumferential speed of the rotor at its largest diameter, or the fact that a rotor is running well above its first critical bending frequency. The requirements on the AMB and the design limitations can be very different.

A record from about 50 years ago are the 300 kHz rotation speed that have been realized in physical experiments for testing the material strength of small steel balls (about 1 to 2 mm in diameter) under centrifugal load . In today's industrial applications rotational speeds that have been realized are in the range of about 3kHz for a grinding spindle, or about 5kHz for small

turbo-machinery. Problems arise from eddy current and hysteresis losses in the magnetic material, air losses, and the related requirements for power generation and adequate heat dissipation if the rotor runs in vacuum.

4 Size

In principle, there appears to be no upper limit for the bearing size, it can be adapted to any load. Problems arising with assembling the bearing lead to special design variations, where the bearing is separated in two halves, or the single magnets are even treated individually.

5 High Temperature AMB

The application of active magnetic bearings (AMBs) for gas turbines and aircraft engines would open large potentials for novel design. In order to utilize the full advantages of active magnetic bearings, operation in gas turbine and aircraft engines requires that the magnetic bearing should work properly at high temperatures. Challenges indesigning such bearings consist in material evaluation, manufacturing process and high temperature displacement sensor development. High temperature active magnetic bearings (HT AMBs) are under development in various places. Operating temperatures of up to 600 ℃ have been reached, at rotor speeds of 50'000 rpm. Such a performance cannot be reached by any other kind of bearing. The soft magnetic materials for stator and rotor are cobalt based alloys such as Hiperco

50 and Hiperco 50-HS, the windings are made of ceramic coated copper wire with high temperature potting materials. Functional tests were quite successful, but the long-term exposure to high temperature needs further research, as the actual results are not yet convincing. In addition, heat dissipation of the internally generated losses under heavy bearing loads have shown to need special attention.

6 Losses

With contact-free rotors there is no friction in the magnetic bearings. The operation of active magnetic bearings causes much less losses than operating conventional ball or journal bearings, but, nevertheless, the losses have to be taken into account, and sometimes they lead to limitations. Losses can be grouped into losses arising in the stationary parts, in the rotor itself, and losses related to the design of the control.Losses in the stationary parts of the bearing come mainly from copper losses in the windings of the stator and from losses in the amplifiers. The copper losses are a heat source, and, if no sufficient cooling is provided, can limit the control current and hence the maximal achievable carrying force, as described before Losses in the rotor part are more complex and lead to more severe limitations. These losses comprise iron lossescaused by hysteresis and eddy currents, and air drag losses. The losses heat up the rotor, cause a breaking torque on therotor, and have to be compensated by the drive power of the motor.

7 Precision

Precision in rotating machinery means most often how precise can the position of the rotor axis be guaranteed. This has consequences for machining tools, and for the surface quality of parts that are being machined by grinding, milling or turning. In addition, the question of how precise can magnetic bearings become in principle, is of interest for applications such as optical devices, optical scanner, wafer stepper, or lithography. These machines and processes are key elements for semiconductor industry. Active magnetic bearings levitate an object, rotating or not, with feedback control of measured displacement sensor signal. The performance of AMB systems is therefore directly affected by the quality of a sensor signal. Precision control is facilitated by the absence of hysteresis and of deformation-prone heat sources, which touches upon material and design aspects.

8 Summary and Expectation

Beside these advantages of AMB, some limitations arise from two reasons, the state of the actual technology in design and material, and from basic physical relations. The further technology will be consider about these and develop this way as well as wider business applications.

Appendix B

Some Key Parameters in This Study

The force-displacement coefficient [N/m] and force-current coefficient [N/A] are as follows:

R=-4375,000

S=3.5028.

The dynamic matrix from the amplitude to the displacement at bearing position and sensor position are:

$$C_{a2b} = \begin{bmatrix} -1.19029 & -0.608354 \\ -1.19029 & 0.608354 \end{bmatrix}$$

$$C_{a2s} = \begin{bmatrix} -1.93745 & -1.83546 \\ -1.93745 & 1.83546 \end{bmatrix}.$$

The dynamic matrix from the states to the displacement at bearing position and sensor positaion are:

$$M_{s2b} = \begin{bmatrix} 1 & -0.1105 & -1.19029 & -0.608354 \\ 1 & 0.1105 & -1.19029 & 0.608354 \end{bmatrix}$$

$$M_{s2s} = \begin{bmatrix} 1 & -0.1317 & -1.19029 & -0.608354 \\ 1 & 0.1317 & -1.19029 & 0.608354 \end{bmatrix}.$$

The system matrix, input matrix, output matrix and direct term matrix are:

$$A = \begin{bmatrix} 0 & 1 & 0 & 0 & 0 & 0 & 0 & 0 & 0 & 0 \\ 28500 & 0 & 0 & 0 & -33900 & 0 & 0 & 0 & 11.9 & 11.9 \\ 0 & 0 & 0 & 1 & 0 & 0 & 0 & 0 & 0 & 0 \\ 0 & 0 & 57200 & 0 & 0 & 0 & 315000 & 0 & -207.1 & -207.1 \\ 0 & 0 & 0 & 0 & 0 & 1 & 0 & 0 & 0 & 0 \\ -33900 & 0 & 0 & 0 & -1270700 & 0 & 0 & 0 & -13.57 & -13.57 \\ 0 & 0 & 0 & 0 & 0 & 0 & 0 & 1 & 0 & 0 \\ 0 & 0 & 1900 & 0 & 0 & 0 & -5739900 & 0 & -6.9289 & 6.9289 \\ 0 & 0 & 0 & 0 & 0 & 0 & 0 & 0 & -4545.5 & 0 \\ 0 & 0 & 0 & 0 & 0 & 0 & 0 & 0 & 0 & -4545.5 \end{bmatrix}$$

$$B = \begin{bmatrix} 0 & 0 & 0 & 0 & 0 & 0 & 0 & 0 & 2840.9 & 0 \\ 0 & 0 & 0 & 0 & 0 & 0 & 0 & 0 & 0 & 2840.9 \end{bmatrix}^T \qquad D = \begin{bmatrix} 0 & 0 \\ 0 & 0 \end{bmatrix}$$

$$C = \begin{bmatrix} 5000.0 & 0 & -658.5 & 0 & -9687.3 & 0 & -9177.3 & 0 & 0 & 0 \\ 5000.0 & 0 & 658.5 & 0 & -9687.3 & 0 & 9177.3 & 0 & 0 & 0 \end{bmatrix}$$

Weighting matrics Q and R in the performamce index, observer design matrics Q_o and R_o, and the SVFB gain matrix K and the observer gain matrix L are as follows:

$$R = \begin{bmatrix} 0.1 & 0 \\ 0 & 0.1 \end{bmatrix} \qquad R_o = \begin{bmatrix} 1 & 0 \\ 0 & 1 \end{bmatrix}$$

$$Q = \begin{bmatrix} 5 & 0 & 0 & 0 & 0 & 0 & 0 & 0 & 0 & 0 \\ 0 & 1 & 0 & 0 & 0 & 0 & 0 & 0 & 0 & 0 \\ 0 & 0 & 5 & 0 & 0 & 0 & 0 & 0 & 0 & 0 \\ 0 & 0 & 0 & 1 & 0 & 0 & 0 & 0 & 0 & 0 \\ 0 & 0 & 0 & 0 & 5 & 0 & 0 & 0 & 0 & 0 \\ 0 & 0 & 0 & 0 & 0 & 1 & 0 & 0 & 0 & 0 \\ 0 & 0 & 0 & 0 & 0 & 0 & 5 & 0 & 0 & 0 \\ 0 & 0 & 0 & 0 & 0 & 0 & 0 & 1 & 0 & 0 \\ 0 & 0 & 0 & 0 & 0 & 0 & 0 & 0 & 1 & 0 \\ 0 & 0 & 0 & 0 & 0 & 0 & 0 & 0 & 0 & 1 \end{bmatrix} \quad Q_o = \begin{bmatrix} 1 & 0 & 0 & 0 & 0 & 0 & 0 & 0 & 0 & 0 \\ 0 & 1 & 0 & 0 & 0 & 0 & 0 & 0 & 0 & 0 \\ 0 & 0 & 1 & 0 & 0 & 0 & 0 & 0 & 0 & 0 \\ 0 & 0 & 0 & 1 & 0 & 0 & 0 & 0 & 0 & 0 \\ 0 & 0 & 0 & 0 & 1 & 0 & 0 & 0 & 0 & 0 \\ 0 & 0 & 0 & 0 & 0 & 1 & 0 & 0 & 0 & 0 \\ 0 & 0 & 0 & 0 & 0 & 0 & 1 & 0 & 0 & 0 \\ 0 & 0 & 0 & 0 & 0 & 0 & 0 & 1 & 0 & 0 \\ 0 & 0 & 0 & 0 & 0 & 0 & 0 & 0 & 1 & 0 \\ 0 & 0 & 0 & 0 & 0 & 0 & 0 & 0 & 0 & 1 \end{bmatrix}$$

$$K = \begin{bmatrix} 4.1511 \times 10^6 & 4.1511 \times 10^6 \\ 2.4227 \times 10^4 & 2.4227 \times 10^4 \\ -4.6531 \times 10^5 & 4.6531 \times 10^5 \\ -1.9437 \times 10^3 & 1.9437 \times 10^3 \\ -1.0926 \times 10^5 & -1.0926 \times 10^5 \\ -6.4738 \times 10^2 & -6.4738 \times 10^2 \\ -1.4594 \times 10^4 & 1.4594 \times 10^4 \\ -1.2079 \times 10^2 & 1.2079 \times 10^2 \\ 1.4466 \times 10^2 & -2.3940 \times 10^1 \\ -2.3940 \times 10^1 & 1.4466 \times 10^2 \end{bmatrix}^T \qquad L = \begin{bmatrix} 32.825 & 32.825 \\ 5601.1 & 5601.1 \\ -362.39 & 362.39 \\ -86727 & 86727 \\ -2.9912 & -2.9912 \\ -896.82 & -896.82 \\ -2.3115 & 2.3115 \\ -1088.4 & 1088.4 \\ 1.7852 \times 10-8 & -4.4922 \times 10-11 \\ -1.4978 \times 10-10 & 1.7750 \times 10-8 \end{bmatrix}$$

Appendix C

Computing Processing of the Matrix in Chapter 2.5

%START
% plant modeling computing

% with a RIGID rotor
% inputs:[F1 F2] ; outpus:[X1 X2] ; state vector: [x0 x0' theta theta']'
a2=[0 1 0 0 ; 0 0 0 0; 0 0 0 1; 0 0 0 0];
b2=[0 0 ; 1/m 1/m; 0 0 ; -(L/2-l)/Io (L/2-l)/Io];

% inputs:[icontrol1 icontrol2]; outpus:[X1 X2];
% state vector: [x0 x0' theta theta']'
a5=[0 1 0 0 ; 2*R/m 0 0 0; 0 0 0 1; 0 0 2*(L/2-l)^2*R/Io 0];
b5=[0 0 ; S/m S/m; 0 0 ; -S*(L/2-l)/Io S*(L/2-l)/Io];
c5=[1 0 -(L/2-l2) 0; 1 0 (L/2-l2) 0];
d5=[0 0 ; 0 0];
%outputs:[Vsensor1 Vsensor2] %inptus:[Vcontrol1 Vcontrol2]
a9=a5; b9=0.25.*b5; c9=5000*c5; d9=d5;

%with a FLEXIBLEe rotor
%inputs:[F1 F2] %outpus:[X1 X2]; state vector: [a1 a1' a2 a2']'
a13tmp=-M^(-1)*K;
b13tmp=M^(-1)*P;
a13=[0 1 0 0 ; a13tmp(1,1) 0 a13tmp(1,2) 0 ;
        0 0 0 1; a13tmp(2,1) 0 a13tmp(2,2) 0] ;
b13=[0 0; b13tmp(1,1) b13tmp(1,2);
        0 0; b13tmp(2,1) b13tmp(2,2)];
c13=[Campl2sen(1,1) 0 Campl2sen(1,2) 0;
        Campl2sen(2,1) 0 Campl2sen(2,2) 0];

%OVERALL characteristcs: flexible + rigid
%inputs:[F1 F2]; outpus:[X1 X2]
%state vector: [x0 x0' theta theta' a1 a1' a2 a2']'

```
atmp=zeros(4);
a14=[a2,atmp;   atmp,a13];
b14=[b2;   b13];
c14=[ 1 0 -(L/2-l2) 0 Campl2sen(1,1) 0 Campl2sen(1,2) 0;
      1 0 (L/2-l2) 0 Campl2sen(2,1) 0 Campl2sen(2,2) 0];
d14=d5;


%inputs:[icontrol1 icontrol2]; outputs:[Vsensor1 Vsensor2]
Mrfv2x=[1 0 -(L/2-l) 0 Campl2b(1,1) 0 Campl2b(1,2) 0;
        1 0 (L/2-l) 0 Campl2b(2,1) 0 Campl2b(2,2) 0];
a15tmp=b14*([R 0; 0 R]*Mrfv2x);
a15=a14+a15tmp;
b15=b14*[S 0;   0 S];
c15=5000*c14;
d15=d5;


%outputs:[Vsensor1 Vsensor2]; inptus:[Vcontrol1 Vcontrol2]
%10 state vectors [x0 x0' theta theta' a1 a1' a2 a2' icontrol1 icontrol2]'
a16tmp=[-1/2.2e-4 0; 0 -1/2.2e-4 ];
b16tmp=[0.25/2.2e-4 0; 0 0.25/2.2e-4 ];


A=[a15 b15; zeros(2,8) a16tmp];
B=[zeros(8,2); b16tmp];
C=5000*[c14 zeros(2,2)];
D=d5;


%END
```

Acknowledgement

A thesis like this is never possible without the help, encouragement, motivation and influence in a large number of people.

Professor Joo Ho Yang, my advisor, taught me many things, most importantly, how to do research and how to write well. Professor Yang is an inexhaustible storehouse of knowledge insight and help on just about any subject. His influence pervades this thesis and I am deeply indebted to him for being my advisor teacher and friend. Thank you.

Tanks to my thesis committee members, Prof. Byung Gun Jung, Prof. Seok Kwon Jeong, Prof. Ji Seong Jang and Prof. Young Bok Kim, influenced the direction of my work and the writing of my thesis in their own ways.

Other than my committee members, I would like to thank Dr. Sheng Ho Shim graduated from my lab for introducing former study in my project and directing me to do experiments.

Thanks to Mr. Hwang Hun Jeong for encouraging and commenting on my ideas and assisting in my work. Thanks to all other coworkers in my lab for interesting discussions and commenting on papers. And the administrative and systems staff in the department went out of their way to make life easy.

And thanks to my Chinese friends and schoolmates, who assisted my work, perfected the language in my thesis presentation and defense, and helped me a lot during the years doing my Ph.D.

My family supported me to continue during the ups and downs leading to this thesis. I am grateful for the support, encouragement and love my family has provided through the years, thank you so much.

Most of all, my beautiful wife and soul mate, Ellen Wang, has patiently endured the pursuit of this Ph.D. and lovingly encouraged me and motivated to finish, I would like to dedicate this paper to her in token of my appreciation and affection.